The Pennsylvania State University

The Graduate School

Department of Aerospace Engineering

MATHEMATICAL MODELS FOR SNAKE ROBOT LOCOMOTION AND GAIT OPTIMIZATION

A Thesis in

Aerospace Engineering

by

Appa Rao Nirakh

Submitted in Partial Fulfillment
of the Requirements
for the Degree of

Master of Science

August 2005

Appa Rao Nirakh

The thesis of Appa Rao Nirakh was reviewed and approved* by the following:

Farhan S. Gandhi
Associate Professor of Aerospace Engineering
Thesis Advisor

Sean N. Brennan
Assistant Professor of Mechanical Engineering

George A. Lesieutre
Professor of Aerospace Engineering
Head of the Department of Aerospace Engineering

*Signatures are on file in the Graduate School

ABSTRACT

The present thesis aims to develop dynamic models suitable for the analysis and design of robotic snakes in the serpentine gait. Specifically, this research presents an implicit model with a high degree of design flexibility, namely the ability to change the number of links and to vary friction characteristics in the model formulation. The implicit model is validated numerically by comparison to an explicit model with small number of links. The validated implicit model is then used to establish the optimal gait for a six-link snake robot that minimizes the energy input while maximizing the kinetic energy of forward locomotion or in other words the gait that maximizes the efficiency of forward locomotion. Buckingham pi theorem is used to combine the various parameters influencing the snake locomotion into a group of dimensionless parameters. The locomotion is analyzed using two solution methods: 1) an iterative search over a range of operational parameters - amplitude of angular displacement inputs at each joint and relative phase lag between the sinusoidal displacement inputs at the joints and 2) a non-linear multi-variable optimization, to determine the optimally efficient gait. Results indicate that, an optimal gait exists that maximizes the efficiency of forward locomotion. The non-linear optimization technique is then used to determine the optimal gait parameters for a range of friction characteristics. Experimental tests are performed on a six-link snake robot. Friction characteristics of the snake robot operating on treadmill are determined and the test results are validated against those established via the analytical model.

Furthermore, a mathematical model for continuum snake robot in serpentine gait is presented based on utilization of the beam bending theory. The gait of continuum model is compared to that of a rigid-link model assuming the total mass, length of the snake, and operational parameters are kept identical. Results indicate that the gait of a six-link articulated snake matches closely to that of a five element continuum snake model. The operational parameters include frequency, magnitude, and phase lag of the moments applied to each segment of the continuum robot. A detailed mathematical formulation of the friction model employed is presented.

TABLE OF CONTENTS

LIST OF FIGURES

LIST OF TABLES

ACKNOWLEDGEMENTS

I would like to sincerely thank my advisors, Dr. Farhan Gandhi and Dr. Sean Brennan for their guidance, support and encouragement during the course of my research. I hope, I have performed close enough to their expectations. I am also thankful to Dr. Lesieutre for agreeing to be on my thesis committee. I am really grateful to Vishisht for helping me out with the experimental set-up. Special thanks to Rupi, Goutham and many others fellow Penn Staters for helping me out in difficult times be it academic or otherwise.

Finally, I would like to thank my family members who have constantly encouraged me and supported me to give my best. My dad especially has been a true source of inspiration.

Chapter 1

INTRODUCTION

1.1 Background and Motivation

Snake robots offer a wide range of applications in areas such as reconnaissance, inspection, exploration etc. Because of their complex motion, it is difficult to analyze snake locomotion with regard to these various application areas to establish the underlying dynamic equations governing serpentine locomotion, determine optimal gait for minimal power consumption, and size on-board power systems to allow snake robots to operate autonomously with limited power supply.

Hirose ([1] - [4]) was the first to analyze snake-like locomotion by performing a series of experiments on actual snakes. These experiments sought to determine the path followed by a snake as it locomotes forward in the serpentine gait, referred to by Hirose as a Serpenoid Curve. Hirose also established that a net forward motion could be generated by applying time-varying torque along the length of the snake. Based on these results, a wheel-based, rigid-link snake-like locomotor was built capable of moving forward using applied joint torques without driving the wheels. This robot, called the Active Cord Mechanism (ACM III), shown in Fig. 1.1 consisted of a series of connected segments, each of which sat upon an actively controlled, rotating wheel base. However, the control of the position and guidance of the snake robot remained a heuristically derived procedure, without the ability to give precise feedback control for this form of

locomotion. The next generation of snake robots built by Hirose (Koryu I and II) were modified to allow vertical motion and exert a rotational torque on its nearest neighbor. Furthermore, the wheels were controlled to move together, thus enabling it to climb stairs and even cross over gaps in the floor. However, the study was purely focused on the kinematics of motion, leaving open issues related to practical determination of gait.

The Robotics group at the California Institute of Technology developed mathematical models and theory ([5] - [8]) to expand the study of the kinematics of snakes to include the dynamics of wheel-based snake-like locomotion. In these models, forward motion is generated by coupling internal shape changes with external holonomic constraints assuming no-slip constraints along the wheel axes. Qualitative experiments were conducted on a 30 degree-of-freedom hyper-redundant robot (Fig. 1.2) that demonstrated locomotion and other applications related to grasping, obstacle avoidance etc. However, there were few quantitative studies confirming the accuracy and results obtained by the mathematical models. Further, the predicted locomotion was not studied with regard to variations in friction characteristics and minimizing the power consumption.

Design and motion planning issues for an articulated mechanical snake robot without wheels built at the University of Michigan are presented in [9]. The motion planning system provides the robot with a basic motion pattern that can be easily modified for different tasks and environments. Each link has a different number of degrees-of-freedom in each motion stage, providing the robot with great adaptability even during contact with obstacles in a cluttered environment. The GMD-snake ([10], [11]) shown in Fig. 1.3 and the snake-like robot presented in [12] utilize motion control

software that enable them to move on different surfaces and to deal with obstacles. Experiments were successfully presented to sense the environment and to react accordingly. A study of the physical modeling and metrics for evaluation of limbless locomotion and the mechanism and control of a 20 degree of freedom snake robot is described by Dowling ([13] and [14]). Multiple gaits are demonstrated including novel non-snake-like gaits. Ma [15] derived the serpentine curve at constant steady-state velocity for the uniform creeping locomotion of the snake by physiologically analyzing its muscle characteristics. A multi-segment robot concept is discussed in [16] for use in space-based construction operations. The notion of shape function is used to position the serpentine robot at a prescribed position and orientation. An *n*-body simulation program is developed based on a Newton-Euler form of the equations of motion of the robot. Motion tests are presented that compare experimental results with pertinent analytical predictions. Experiments are performed by Nilsson [17] to demonstrate serpentine locomotion on uniform surfaces. Theoretical kinematical analysis is then presented to explain the experimental findings. A biologically based underwater, autonomous vehicle based on the sea lamprey which swims by rhythmic lateral undulations of the body axis is presented in [18].

The above studies have provided insight into the mathematical modeling of the kinematics and dynamics as well as dealing with issues related to the experimental synthesis of serpentine locomotion. However, issues remain with these models including questions about the level of mathematical complexity, little if any validation against experimental results, differing assumptions regarding robot/ground interaction, and

limited analysis of power consumption as a function of gait parameters, operating speed, etc.

Iwasaki [19] and his colleagues recently investigated robotic snake gaits that achieve forward locomotion at a prescribed speed while requiring the least power. Their mathematical model assumed a multi-link robotic snake without wheels. However, this model was not validated experimentally to confirm the optimal gait parameters established via analytical results.

The aforementioned studies analyzed and synthesized the serpentine locomotion as an articulated mechanism, modeling the snake robot as a series of rigid links. In general, these snakes had wheels mounted underneath each rigid link. Unfortunately, such wheel-based robots would not be best suited for rugged or muddy environments, and the inflexibility of rigid links does not allow the range of motion for which snake robots are designed. Besides offering better terrain adaptability than the conventional rigid-link designs, flexible robots that can actually emulate the snakes creeping motion are highly redundant and robust. However, a continuum dynamic motion requires a more novel approach than rigid robots.

There have been many studies in the field of continuum robots ([20] - [25]), though none directly relates to serpentine locomotion. While some have developed beam-based models to realize robotic mechanisms similar to the elephant trunk, tentacles or tongues of animal, there has been no research prior to this study that focuses on a continuum dynamic description of a snake robot.

1.2 Present Study

The present study aims to address issues seen in previous studies to specifically develop dynamic models suitable for the analysis, design and control of robotic snakes. Specifically, this research seeks to develop an easily modifiable model which has flexibility with respect to number of links as well as the ability to change the friction model. Furthermore, a beam-based continuum formulation of the governing dynamics of snake motion is presented. The objectives of the present study are:

1. To provide a basic framework that allows study of the dynamics of planar serpentine locomotion of a discrete robotic snake model.
2. To determine the operational parameters which optimize the gait of a six-link articulated snake robot to achieve maximum performance index.
3. To experimentally validate the optimal gait results established via the mathematical analysis.
4. To provide a mathematical realization of the continuum snake robot in serpentine gait by deriving the equations of motion describing the dynamics of the continuum snake based on beam finite elements.
5. To compare the gait and locomotion achieved by the continuum snake to that generated by the dynamics of an articulated wheel-based snake robot model.

Chapter 2 deals with the mathematical modeling and analysis of the dynamics of a three-link articulated snake model in two different methods: 1) a closed-form solution approach hereafter referred to as the explicit formulation and 2) an approach where link-to-link joint forces at a present time step are approximated using prior trajectories, an

approach hereafter referred to as an implicit formulation. A comparison of the two proposed methods is then presented to confirm that the implicit and explicit formulations are mathematically equivalent.

The issue of optimal gait resulting in maximum performance index for a six-link robotic snake is studied in Chapter 3. Dimensional analysis and Buckingham pi theorem are used to simplify the analysis by combining the physical variables influencing the system's characteristics into dimensionless groups. An iterative search through a range of the operating parameters is first undertaken to determine whether an optimum exists and is unique. Then, a multi-variable optimization scheme is employed to determine the optimal gait parameters of the snake operating on surfaces with varying friction characteristics and simulation results are summarized. Furthermore, the results predicted by the present study are compared to an earlier study, [**19**].

In Chapter 4, experimental results based on the tests performed on a six-link wheel-based robot are presented. The friction characteristics of snake robot operating on a treadmill are presented. Further, optimal gait is predicted using the multi-variable optimization scheme for the experimental friction model and is compared to the test results.

The mathematical modeling of the dynamics of a continuum snake robot based on beam bending theory is presented in Chapter 5. The gait and locomotion patterns of the continuum model are compared to that of the rigid-link model established in Chapter 3. Finally, Chapter 6 summarizes the main results and important conclusions drawn from the study as well as the scope for future work based on the present models.

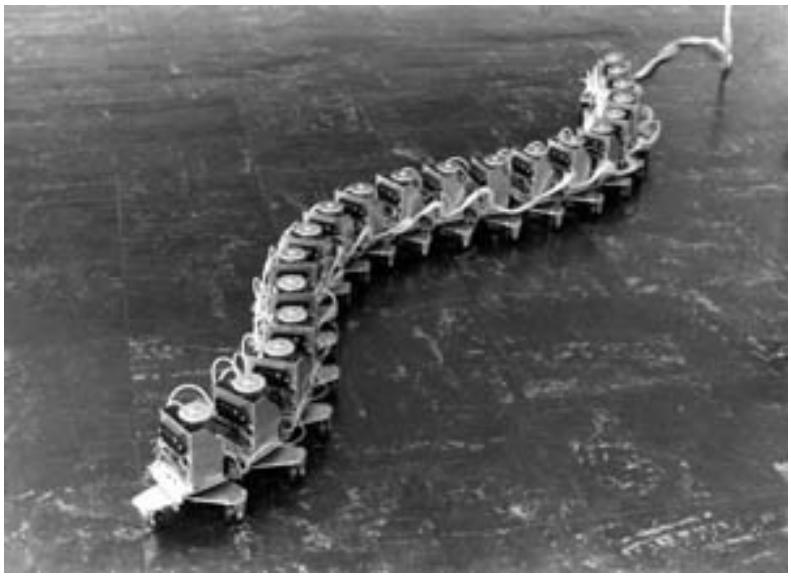

Figure **1.1**: The Active Cord Mechanism (ACM III)

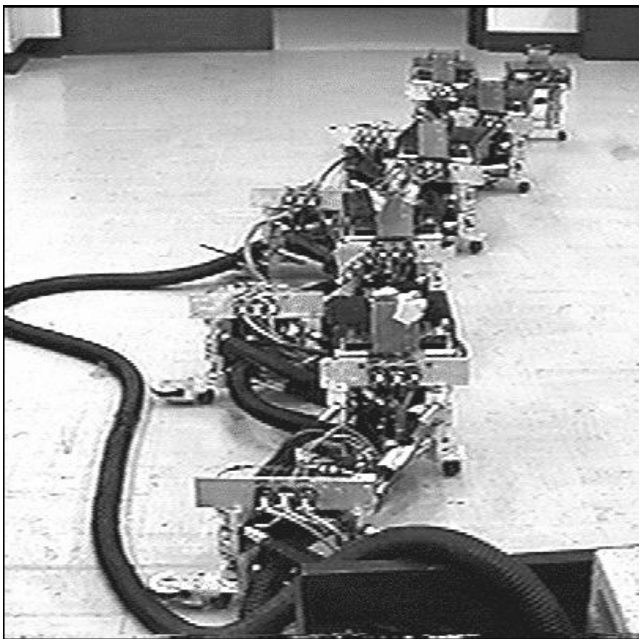

Figure **1.2**: The 30 degree of freedom planar hyper-redundant manipulator

Figure **1.3**:The GMD-Snake

Chapter 2

ARTICULATED SNAKE ROBOT MODEL

2.1 Mathematical Modeling and Analysis

For a snake robot, the key to generating forward locomotion is to exploit different friction coefficients in the normal and tangential directions to the snake at the link-to-ground contact points. As convention, the normal direction is perpendicular to the link and the tangential direction is along the length of the link. Most of the studies ([9], [15], [19], [1] - [4]) assume the normal friction coefficient to be much larger than the tangential friction coefficient; with some ([7] and [8]) assuming that slip in the lateral direction is negligible.

Analytical models of a general robotic snake usually consist of n rigid links actuated at the (n–1) joints connecting these links. Each link is generally assumed to have one point of contact with the ground at its center of gravity, an assumption also made in the present study. Additionally, the following assumptions are made within this study to derive the equations of motion of a snake robot:

- Each link has uniform mass distribution and the parameters for each link - length, mass etc. - are identical for all the links.
- A viscous friction model is employed to describe link-to-ground interaction. The friction coefficients in the normal and tangential direction are assumed constant over the entire snake. Viscous friction is governed by: $F_{visc} = -c \cdot v$; where v is

the velocity in a particular direction, c, the viscous friction coefficient in that direction, and F_{visc}, the friction induced force at the point of contact.

- Only planar serpentine locomotion is considered.

The general robotic snake system consists of a total of $n + 2$ degrees of freedom with two degrees of freedom representing the planar position of the center of mass of the first link and the remaining degrees of freedom representing the orientations of the n links in the global reference frame.

2.1.1 Explicit Formulation for a three-link robotic snake

To illustrate the mathematical formulation of an explicit model, a three-link model is considered as it is the simplest rigid-link snake robot that can locomote. The five independent degrees of freedom for a three-link model are - $x, y, \theta_1, \theta_2, \theta_3$. A schematic of the model is shown in Fig. **2.1** and a free-body diagram indicating the forces and moments acting on each link is shown in Fig. **2.2**. The force and moment equilibrium equations: $\sum F_{x,i} = m_i \ddot{x}_i$, $\sum F_{y,i} = m_i \ddot{y}_i$ and $\sum M_{z,i} = I_i \ddot{\theta}_i$ for each of the three links can be written as follows:

Link 1

$$F_{g,1}{}^{x} + F_{1x} = m\ddot{x}_1 \tag{2.1}$$

$$F_{g,1}{}^{y} + F_{1y} = m\ddot{y}_1 \tag{2.2}$$

$$T_1 - F_{1x} l \sin\theta_1 + F_{1y} l \cos\theta_1 = I_c \ddot{\theta}_1 \tag{2.3}$$

Link 2:

$$-F_{1x} + F_{g,2}{}^{x} + F_{2x} = m\ddot{x}_2 \tag{2.4}$$

$$-F_{1y} + F_{g,2}{}^{y} + F_{2y} = m\ddot{y}_2 \tag{2.5}$$

$$(T_2 - T_1) - (F_{1x} + F_{2x})l\sin\theta_2 + (F_{1y} + F_{2y})l\cos\theta_2 = I_c\ddot{\theta}_2 \tag{2.6}$$

Link 3:

$$-F_{2y} + F_{g,3}{}^{y} = m\ddot{y}_3 \tag{2.7}$$

$$-F_{2y} + F_{g,3}{}^{y} = m\ddot{y}_3 \tag{2.8}$$

$$-T_2 - F_{2x}l\sin\theta_3 + F_{2y}l\cos\theta_3 = I_c\ddot{\theta}_3 \tag{2.9}$$

where the parameters are defined as follows:

m	Mass of each link
l	Distance from the center of gravity of the link to the joint, equal to half of the link length assuming uniform mass distribution
I_c	Mass moment of inertia of the link about the center of mass
x_i, y_i, θ_i	The global position and orientation of the i^{th} link
T_i	Torque applied at the i^{th} joint (between i^{th} and $(i+1)^{th}$ links)
$F_{g,i}{}^{x}, F_{g,i}{}^{y}$	Frictional forces between the i^{th} link and the ground at the center of gravity in the global coordinate system, resolved in the x and y directions.
F_{ix}, F_{iy}	The joint forces between i^{th} and $(i+1)^{th}$ links in the global coordinate

system, resolved in the x and y directions

To obtain the time-varying positions and orientations of the various links, Eqs. (**2.1** - **2.9**) have to be solved simultaneously. Two solution methods, namely explicit and implicit, are considered in this study. The explicit method utilizes the exact model without any approximations. The force and moment dynamic equations are simplified by rearranging them to eliminate the joint forces. These equations are further simplified by enforcing the compatibility conditions that describe the positions of the links in terms of the five independent variables $x, y, \theta_1, \theta_2, \theta_3$. The resulting number of governing equations is always equal to the number of independent degrees of freedom; hence this solution method is hereafter referred to as an explicit method.

The challenge with the explicit model formulation is that the joint force and compatibility algebraic equations are highly nonlinear, making it difficult to write the governing differential equations in only the independent variables. One can overcome this algebraic difficulty by allowing more system differential equations than are necessary, e.g. by approximating the joint connections by spring-damper systems. The dynamics of the system are simulated individually for each link without the necessity of algebraic solutions for the joint forces. Further, the algebraic compatibility conditions are also not needed in the solution method. Because there are more equations than the number of independent degrees of freedom, this solution method is hereafter referred to as an implicit method. These distinctions between explicit and implicit formulations are best illustrated by direct comparison, shown in the following sections.

As an illustration, the explicit equations of motion for a three-link snake are now derived. From Fig. **2.1**, the coordinates of the center of mass of each link can be

expressed as a function of the aforementioned five independent variables, $x, y, \theta_1, \theta_2, \theta_3$ as follows:

$$x_1 = x \tag{2.10}$$

$$y_1 = y \tag{2.11}$$

$$x_2 = x + l \cdot \cos\theta_1 + l \cdot \cos\theta_2 \tag{2.12}$$

$$y_2 = y + l \cdot \sin\theta_1 + l \cdot \sin\theta_2 \tag{2.13}$$

$$x_3 = x + l \cdot \cos\theta_1 + 2l \cdot \cos\theta_2 + l \cdot \cos\theta_3 \tag{2.14}$$

$$y_3 = y + l \cdot \sin\theta_1 + 2l \cdot \sin\theta_2 + l \cdot \sin\theta_3 \tag{2.15}$$

Differentiating Eqs. (**2.10** - **2.15**) with respect to time yields the velocities of the center of mass of the links in the global coordinate system as:

$$\dot{x}_1 = \dot{x} \tag{2.16}$$

$$\dot{y}_1 = \dot{y} \tag{2.17}$$

$$\dot{x}_2 = \dot{x} - l\dot{\theta}_1 \sin\theta_1 - l\dot{\theta}_2 \sin\theta_2 \tag{2.18}$$

$$\dot{y}_2 = \dot{y} + l\dot{\theta}_1 \cos\theta_1 + l\dot{\theta}_2 \cos\theta_2 \tag{2.19}$$

$$\dot{x}_3 = \dot{x} - l\dot{\theta}_1 \sin\theta_1 - 2l\dot{\theta}_2 \sin\theta_2 - l\dot{\theta}_3 \sin\theta_3 \tag{2.20}$$

$$\dot{y}_3 = \dot{y} + l\dot{\theta}_1 \cos\theta_1 + 2l\dot{\theta}_2 \cos\theta_2 + l\dot{\theta}_3 \cos\theta_3 \tag{2.21}$$

Similarly, differentiating the velocities i.e. Eqs. (**2.16** - **2.21**) with respect to time yields the accelerations of the center of mass of the links as:

$$\ddot{x}_1 = \ddot{x} \tag{2.22}$$

$$\ddot{y}_1 = \ddot{y} \tag{2.23}$$

$$\ddot{x}_2 = \ddot{x} - l\ddot{\theta}_1 \sin\theta_1 - l\ddot{\theta}_2 \sin\theta_2 - l\dot{\theta}_1^{\,2} \cos\theta_1 - l\dot{\theta}_2^{\,2} \cos\theta_2 \tag{2.24}$$

$$\ddot{y}_2 = \ddot{y} + l\ddot{\theta}_1 \cos\theta_1 + l\ddot{\theta}_2 \cos\theta_2 - l\dot{\theta}_1^{\,2} \sin\theta_1 - l\dot{\theta}_2^{\,2} \sin\theta_2 \tag{2.25}$$

$$\ddot{x}_3 = \ddot{x} - l\ddot{\theta}_1 \sin\theta_1 - 2l\ddot{\theta}_2 \sin\theta_2 - l\ddot{\theta}_3 \sin\theta_3 - l\dot{\theta}_1^{\,2} \cos\theta_1 - 2l\dot{\theta}_2^{\,2} \cos\theta_2 - l\dot{\theta}_3^{\,2} \cos\theta_3 \tag{2.26}$$

$$\ddot{y}_3 = \ddot{y} + l\ddot{\theta}_1 \cos\theta_1 + 2l\ddot{\theta}_2 \cos\theta_2 + l\ddot{\theta}_3 \cos\theta_3 - l\dot{\theta}_1^{\,2} \sin\theta_1 - 2l\dot{\theta}_2^{\,2} \sin\theta_2 - l\dot{\theta}_3^{\,2} \sin\theta_3 \tag{2.27}$$

The contact forces between the ground and the link at the center of mass are modeled assuming the viscous friction model stated previously. The friction coefficients and hence the contact forces are defined locally i.e. in the normal and tangential directions and then transformed back into the global coordinate system. With reference to Fig. **2.3**, the contact forces in the tangential and normal directions can be written using the viscous friction model described earlier as:

$$F_{g,i}{}^{t} = -C_i^{\,t} \cdot v_i^{\,t} = -C_i^{\,t} \cdot \left(\dot{x}_i \cos\theta_i + \dot{y}_i \sin\theta_i\right) \tag{2.28}$$

$$F_{g,i}{}^{n} = -C_i^{\,n} \cdot v_i^{\,n} = -C_i^{\,n} \cdot \left(-\dot{x}_i \sin\theta_i + \dot{y}_i \cos\theta_i\right) \tag{2.29}$$

where C_t and C_n are the tangential and normal friction coefficients respectively. Equations (**2.28** - **2.29**) can be expressed in matrix form as follows:

$$\begin{Bmatrix} {F_{g,i}}^t \\ {F_{g,i}}^n \end{Bmatrix} = -\begin{bmatrix} {C_i}^t & 0 \\ 0 & {C_i}^n \end{bmatrix} \cdot \begin{bmatrix} \cos\theta_i & \sin\theta_i \\ -\sin\theta_i & \cos\theta_i \end{bmatrix} \cdot \begin{Bmatrix} \dot{x}_i \\ \dot{y}_i \end{Bmatrix} \tag{2.30}$$

The contact forces in the normal and tangential directions can be transformed back into the global coordinate system as follows:

$${F_{g,i}}^x = {F_{g,i}}^t \cos\theta_i - {F_{g,i}}^n \sin\theta_i \tag{2.31}$$

$${F_{g,i}}^y = {F_{g,i}}^t \sin\theta_i + {F_{g,i}}^n \cos\theta_i \tag{2.32}$$

Using Eqs. (**2.30** - **2.32**) the friction forces associated with the i^{th} link can be expressed in the global coordinate system as:

$$\begin{Bmatrix} {F_{g,i}}^x \\ {F_{g,i}}^y \end{Bmatrix} = -\begin{bmatrix} \cos\theta_i & -\sin\theta_i \\ \sin\theta_i & \cos\theta_i \end{bmatrix} \cdot \begin{bmatrix} {C_i}^t & 0 \\ 0 & {C_i}^n \end{bmatrix} \cdot \begin{bmatrix} \cos\theta_i & \sin\theta_i \\ -\sin\theta_i & \cos\theta_i \end{bmatrix} \cdot \begin{Bmatrix} \dot{x}_i \\ \dot{y}_i \end{Bmatrix} \tag{2.33}$$

Equations (**2.10** – **2.33**) describe how the compatibility constraints and frictional forces enter the dynamic model. It is now possible to write the governing differential equations, with the first goal to eliminate joint forces. One can eliminate several coupling forces by summing Eqs. (**2.1**), (**2.4**), and (**2.7**):

$$m\left(\ddot{x}_1 + \ddot{x}_2 + \ddot{x}_3\right) = {F_{g,1}}^x + {F_{g,2}}^x + {F_{g,3}}^x \tag{2.34}$$

Similarly, summing Eqs. (**2.2**), (**2.5**), and (**2.8**) results in:

$$m\left(\ddot{y}_1 + \ddot{y}_2 + \ddot{y}_3\right) = {F_{g,1}}^y + {F_{g,2}}^y + {F_{g,3}}^y \tag{2.35}$$

The joint forces, F_{ix} and F_{iy}, are to be eliminated from Eqs. (**2.3**), (**2.6**) and (**2.9**) to obtain the remaining governing equations. This is achieved by expressing the joint

forces in terms of known quantities. Summing Eqs. (**2.4**), (**2.7**) and (**2.5**), (**2.8**) and solving for F_{1x} and F_{1y} respectively results in:

$$-F_{1x} = m(\ddot{x}_2 + \ddot{x}_3) - \left(F_{g,2}{}^{x} + F_{g,3}{}^{x}\right) \tag{2.36}$$

$$-F_{1y} = m(\ddot{y}_2 + \ddot{y}_3) - \left(F_{g,2}{}^{y} + F_{g,3}{}^{y}\right) \tag{2.37}$$

Solving Eqs. (**2.7**) and (**2.8**) for F_{2x} and F_{2y} yields:

$$-F_{2x} = m\ddot{x}_3 - F_{g,3}{}^{x} \tag{2.38}$$

$$-F_{2y} = m\ddot{y}_3 - F_{g,3}{}^{y} \tag{2.39}$$

The right hand side of Eqs. (**2.34**) and (**2.35**) can be expressed solely in terms of the independent variables using the generalized Eq. (**2.33**) and Eqs. (**2.16** - **2.21**). The resulting differential equations will be functions of linear and angular displacements and velocities of the center of mass of the links. The left hand side of Eqs. (**2.34**) and (**2.35**) can be rewritten in terms of the independent variables and their derivatives alone using Eqs. (**2.22** - **2.27**). These equations, upon simplification, yield:

$$\begin{aligned} 3m\ddot{x} - ml\left(2\ddot{\theta}_1 \sin\theta_1 + \ddot{\theta}_2 \sin\theta_2 + \ddot{\theta}_3 \sin\theta_3\right) \\ = Q_1 + ml\left(2\dot{\theta}_1{}^2 \cos\theta_1 + 3\dot{\theta}_2{}^2 \cos\theta_2 + \dot{\theta}_3{}^2 \cos\theta_3\right) \end{aligned} \tag{2.40}$$

$$\begin{aligned} 3m\ddot{y} + ml\left(2\ddot{\theta}_1 \cos\theta_1 + 3\ddot{\theta}_2 \cos\theta_2 + \ddot{\theta}_3 \cos\theta_3\right) \\ = Q_2 + ml\left(2\dot{\theta}_1{}^2 \sin\theta_1 + 3\dot{\theta}_2{}^2 \sin\theta_2 + \dot{\theta}_3{}^2 \sin\theta_3\right) \end{aligned} \tag{2.41}$$

where, Q_1 and Q_2 are defined as:

$$Q_1 = {F_{g,1}}^x + {F_{g,2}}^x + {F_{g,3}}^x \tag{2.42}$$

$$Q_2 = {F_{g,1}}^y + {F_{g,2}}^y + {F_{g,3}}^y \tag{2.43}$$

Substituting Eqs. (2.36) and (2.37) into Eq. (2.3) and simultaneously using Eqs. (2.22 - 2.27) and simplifying results in:

$$\begin{aligned} I_{01}\ddot{\theta}_1 + 2ml\left(\ddot{y}\cos\theta_1 - \ddot{x}\sin\theta_1\right) + ml^2\left[3\ddot{\theta}_2\cos(\theta_1-\theta_2) + \ddot{\theta}_3\cos(\theta_3-\theta_1)\right] \\ = Q_3 + ml^2\left\{-3\dot{\theta}_2{}^2\sin(\theta_1-\theta_2) + \dot{\theta}_3{}^2\sin(\theta_3-\theta_1)\right\} \end{aligned} \tag{2.44}$$

where, Q_3 is defined as:

$$Q_3 = -\left({F_{g,2}}^x + {F_{g,3}}^x\right)l\sin\theta_1 + \left({F_{g,2}}^y + {F_{g,3}}^y\right)l\cos\theta_1 \tag{2.45}$$

Similarly, using Eqs. (2.36 - 2.39) in Eq. (2.6) and simplifying utilizing Eqs. (2.22 - 2.27) yields:

$$\begin{aligned} I_{02}\ddot{\theta}_2 + 3ml\left(\ddot{y}\cos\theta_2 - \ddot{x}\sin\theta_2\right) + ml^2\left[3\ddot{\theta}_2\cos(\theta_1-\theta_2) + 2\ddot{\theta}_3\cos(\theta_2-\theta_3)\right] \\ = Q_4 + ml^2\left\{3\dot{\theta}_1{}^2\sin(\theta_1-\theta_2) - 2\dot{\theta}_3{}^2\sin(\theta_2-\theta_3)\right\} \end{aligned} \tag{2.46}$$

where, Q_4 is defined as:

$$Q_4 = -\left({F_{g,2}}^x + 2{F_{g,3}}^x\right)l\sin\theta_2 + \left({F_{g,2}}^y + 2{F_{g,3}}^y\right)l\cos\theta_2 \tag{2.47}$$

Finally, using Eqs. (2.22 - 2.27) and Eqs. (2.38) and (2.39) in Eq. (2.9) and simplifying yields the last of the five governing equations as:

$$\begin{aligned} I_{03}\ddot{\theta}_3 + ml\left(\ddot{y}\cos\theta_3 - \ddot{x}\sin\theta_3\right) + ml^2\left[\ddot{\theta}_1\cos(\theta_3-\theta_1) + 2\ddot{\theta}_2\cos(\theta_2-\theta_3)\right] \\ = Q_5 + ml^2\left\{-\dot{\theta}_1{}^2\sin(\theta_3-\theta_1) + 2\dot{\theta}_2{}^2\sin(\theta_2-\theta_3)\right\} \end{aligned} \tag{2.48}$$

where Q_5 is defined as:

$$Q_5 = -{F_{g,3}}^x l\sin\theta_3 + {F_{g,3}}^y l\cos\theta_3 \tag{2.49}$$

Equations (**2.40**), (**2.41**), (**2.44**), (**2.46**), and (**2.48**) are the five equations governing the dynamics of a three-link articulated robot. Rewriting these equations in matrix form yields:

$$\begin{bmatrix} 3m & 0 & -2ml\sin\theta_1 & -3ml\sin\theta_2 & -ml\sin\theta_3 \\ 0 & 3m & 2ml\cos\theta_1 & 3ml\cos\theta_2 & ml\cos\theta_3 \\ -2ml\sin\theta_1 & 2ml\cos\theta_1 & I_{01} & 3ml^2\cos(\theta_1-\theta_2) & ml^2\cos(\theta_3-\theta_1) \\ -3ml\sin\theta_2 & 3ml\cos\theta_2 & 3ml^2\cos(\theta_1-\theta_2) & I_{02} & 2ml^2\cos(\theta_2-\theta_3) \\ -ml\sin\theta_3 & ml\cos\theta_3 & ml^2\cos(\theta_3-\theta_1) & 2ml^2\cos(\theta_2-\theta_3) & I_{03} \end{bmatrix}$$

$$\times \begin{Bmatrix} \ddot{x} \\ \ddot{y} \\ \ddot{\theta}_1 \\ \ddot{\theta}_2 \\ \ddot{\theta}_3 \end{Bmatrix} = \begin{bmatrix} 0 \\ 0 \\ T_1 \\ T_2 - T_1 \\ -T_2 \end{bmatrix} + \begin{bmatrix} ml(2\dot{\theta}_1^{\,2}\cos\theta_1 + 3\dot{\theta}_2^{\,2}\cos\theta_2 + \dot{\theta}_3^{\,2}\cos\theta_3) \\ ml(2\dot{\theta}_1^{\,2}\sin\theta_1 + 3\dot{\theta}_2^{\,2}\sin\theta_2 + \dot{\theta}_3^{\,2}\sin\theta_3) \\ ml^2[-3\dot{\theta}_2^{\,2}\sin(\theta_1-\theta_2) + \dot{\theta}_3^{\,2}\sin(\theta_3-\theta_1)] \\ ml^2[3\dot{\theta}_1^{\,2}\sin(\theta_1-\theta_2) - 2\dot{\theta}_3^{\,2}\sin(\theta_2-\theta_3)] \\ ml^2[-\dot{\theta}_1^{\,2}\sin(\theta_3-\theta_1) + 2\dot{\theta}_2^{\,2}\sin(\theta_2-\theta_3)] \end{bmatrix} + \begin{bmatrix} Q_1 \\ Q_2 \\ Q_3 \\ Q_4 \\ Q_5 \end{bmatrix} \quad \textbf{(2.50)}$$

The above equation is of the form $A(X)\cdot\ddot{X} = f(X,\dot{X})$ or $\ddot{X} = g(X,\dot{X})$. These simplified equations can be solved numerically. In this study the MATLAB Simulink software is used to numerically integrate Eq. (**2.50**) to obtain a solution $X(t)$.

Solution methods describing the kinematics and dynamics of the serpentine locomotion resembling the above explicit method detailed have been presented in the literature by many researchers ([**9**], [**11**] - [**17**], and [**4**] - [**8**]). Although the solution methods differ, they all share an ultimate goal of obtaining the time-varying positions and orientations of the links.

2.1.2 Implicit Formulation for a three-link robotic snake

While it is relatively easy to solve for the explicit equations of motion for a three-link model, it is algebraically quite challenging and tedious to solve for the nonlinear equations for snakes with even a moderate number of links. The implicit method simplifies the algebraic manipulations considerably by relaxing an algebraic constraint of connection between the joints and instead modeling them by spring-damper systems. The damper and spring are designed to have vibration dynamics several orders of magnitude faster than the snake's gross motion and therefore this motion should not greatly affect the predicted motion of the snake. This assumption is tested in later sections of this study.

Although replacing each joint's algebraic constraints with joint dynamics greatly increases the order of the dynamic model, it greatly simplifies the necessary mathematical manipulations. Specifically, the positions, velocities and accelerations of the center of mass of the links need not be expressed in terms of the position of the center of mass of the first link, orientations of the links, e.g. in $x, y, \theta_1, \theta_2, \theta_3$, and their derivatives. The original snake consisting of one articulated *n*-link body is therefore deconstructed into *n* coupled but independent bodies. The dynamics of the spring-damper system can be simulated to directly obtain the coupling forces between joints while simultaneously solving for the dynamics of the collective robot snake system. Thus, this method does not even require solving for the joint forces as in the explicit method.

The primary disadvantage of the implicit method over the explicit is that the additional differential equations greatly increase the required simulation time. With the

steady and exponential increase in desktop computing capability, this tradeoff is increasingly unimportant.

To model the joint connections by spring-damper systems, the spring stiffness and damping constant need to be chosen. The spring stiffness is chosen such that the joints are stiff enough to exhibit very fast dynamics and damping constant is chosen to have as minimal vibration as possible. All locomotion torques at each joint are assumed to span the joint such that an equal and opposite torque acts on each link. From Fig. **2.4**, the expressions for the joint forces at i^{th} joint can be written as:

$$F_{ix} = k_i \cdot \left(x^i{}_{i+1} - x^i{}_i \right) + c_i \cdot \left(\dot{x}^i{}_{i+1} - \dot{x}^i{}_i \right) \tag{2.51}$$

$$F_{iy} = k_i \cdot \left(y^i{}_{i+1} - y^i{}_i \right) + c_i \cdot \left(\dot{y}^i{}_{i+1} - \dot{y}^i{}_i \right) \tag{2.52}$$

where the parameters are defined as follows:

k_i	Spring stiffness
c_i	Damping constant
$x^i{}_{i+1}, y^i{}_{i+1}$	Coordinates of the i^{th} joint expressed as a function of the coordinates of the $(i+1)^{th}$ link's center of mass
$x^i{}_i, y^i{}_i$	Coordinates of the i^{th} joint expressed as a function of the coordinates of the i^{th} link's center of mass

The coordinates $x^i{}_i$, $y^i{}_i$, $x^i{}_{i+1}$, and $y^i{}_{i+1}$ can be expressed in terms of the coordinates of the centers of mass of i^{th} and $(i+1)^{th}$ links as:

$$x^{i}_{i+1} = x_{i+1} - l \cdot \cos\theta_{i+1} \quad (2.53)$$

$$x^{i}_{i} = x_{i} + l \cdot \cos\theta_{i} \quad (2.54)$$

$$y^{i}_{i+1} = y_{i+1} - l \cdot \sin\theta_{i+1} \quad (2.55)$$

$$y^{i}_{i} = y_{i} + l \cdot \sin\theta_{i} \quad (2.56)$$

The time derivatives of the positions, i.e. $\dot{x}^{i}_{i}$, $\dot{y}^{i}_{i}$, $\dot{x}^{i}_{i+1}$, and $\dot{y}^{i}_{i+1}$ are obtained by differentiating Eqs. (**2.53** - **2.56**), which are obtained numerically using velocities from the previous time steps. Besides Eqs. (**2.51** - **2.56**), the friction formulation equations, i.e. Eqs. (**2.28** - **2.33**) as established in the explicit formulation are also needed. A key advantage of the implicit method is that the friction model is not inter-linked with the formulation or derivation of the system dynamics. This is quite unlike the explicit model where the governing differential equations have to be re-derived to account for the changes in friction characteristics.

With the joint and contact forces known, the implicit method is easily solved numerically. Eqs. (**2.1** - **2.9**) are integrated using the MATLAB Simulink software to determine the positions and velocities of the center of mass of each link. A flowchart describing the implementation of implicit model in Simulink is presented in Fig. **2.5**.

2.2 Comparison of Implicit and Explicit Formulation Results

To confirm that the implicit and explicit formulations are mathematically equivalent, a three-link snake model is constructed using both methods. The relative errors in the rotations and velocities are compared. The time-step used for the simulations is 0.001s. This was found to be sufficiently small as smaller time steps resulted in only a maximum of 0.1% or less error.

Figures **2.6**, **2.7** and **2.8** represent the relative errors between the implicit and explicit angular displacement and translational velocities of the tail link i.e. link 1 for a three-link snake robot. It appears from these plots that the magnitude of the difference between the two models is quite small (order of 10^{-3}) as compared to the magnitude of motion ($\pi/6$). Similar plots are obtained for the other two links. Such results suggest very close agreement between the two methods.

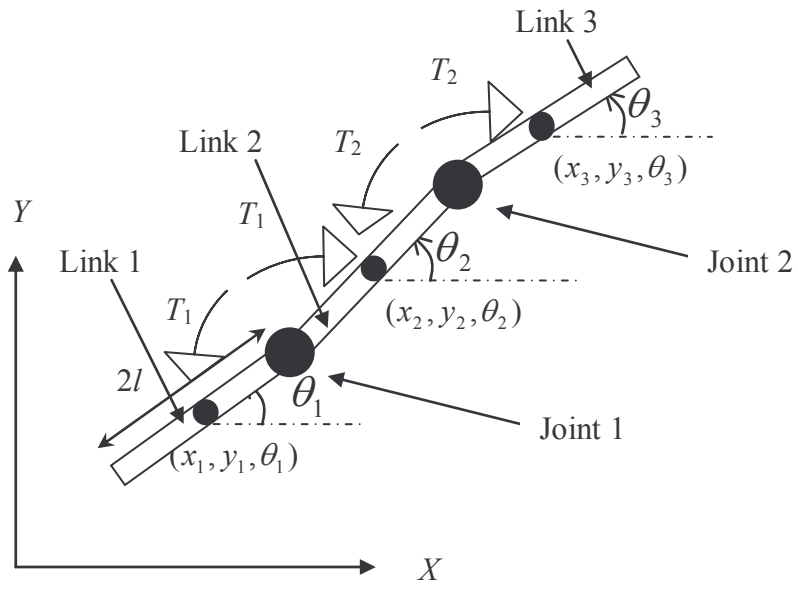

Figure **2.1**: Schematic of a three-link articulated snake model

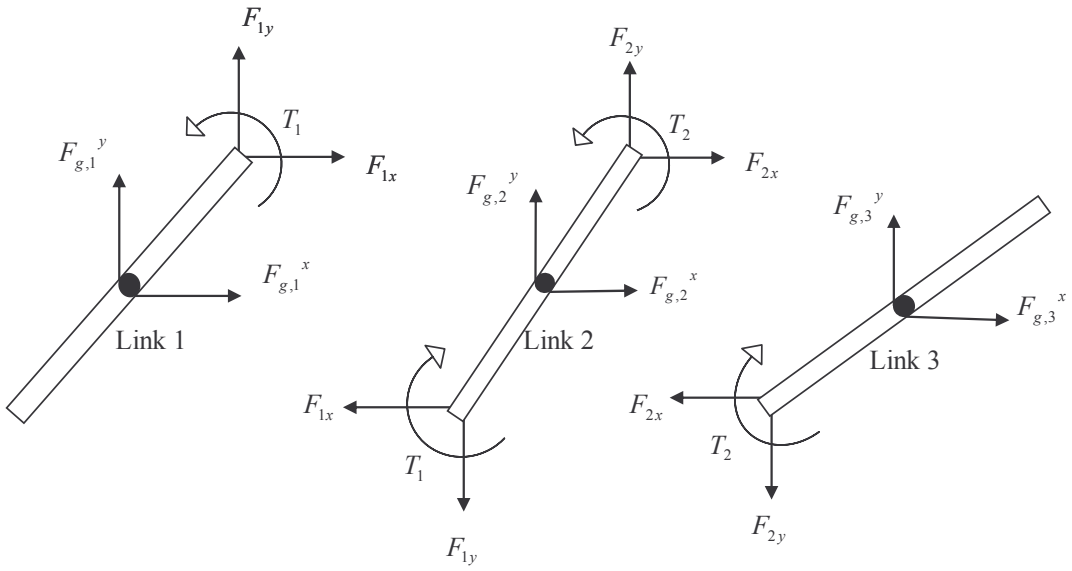

Figure **2.2**: Free-body diagram of the three-link model

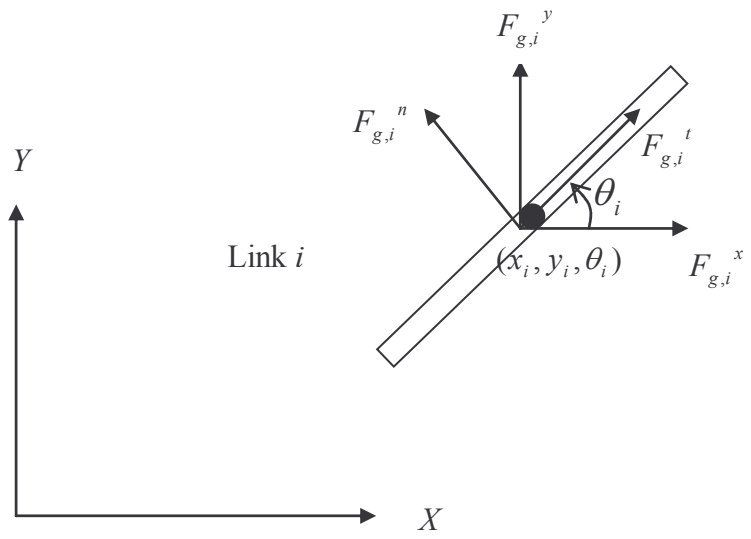

Figure **2.3**: Representation of frictional forces on a generic link

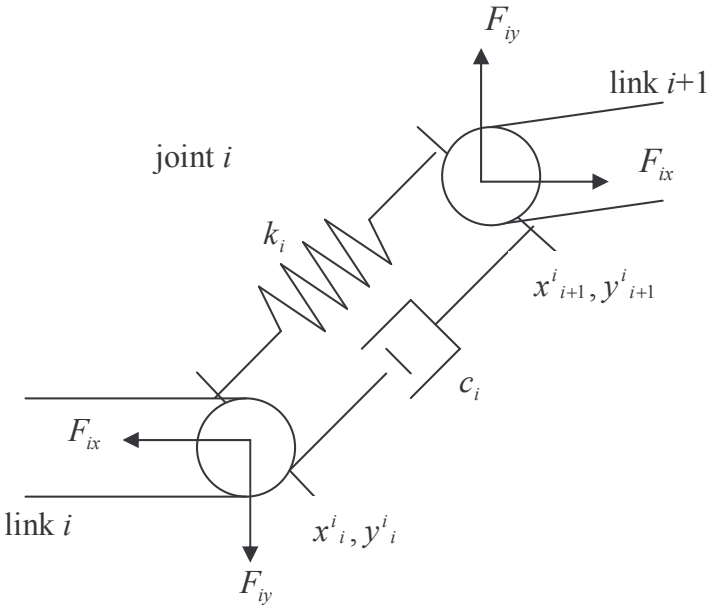

Figure **2.4**: Representation of spring-damper system at the i^{th} joint

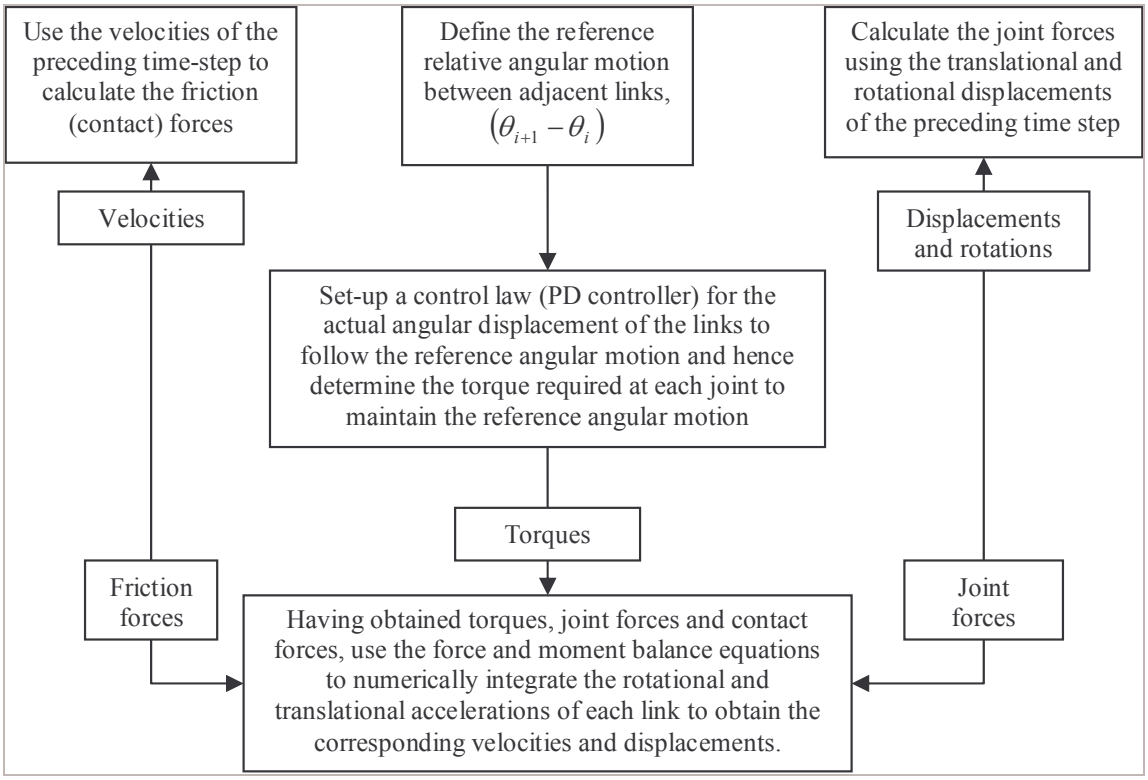

Figure **2.5**: Flowchart representing the implementation of implicit formulation in Simulink

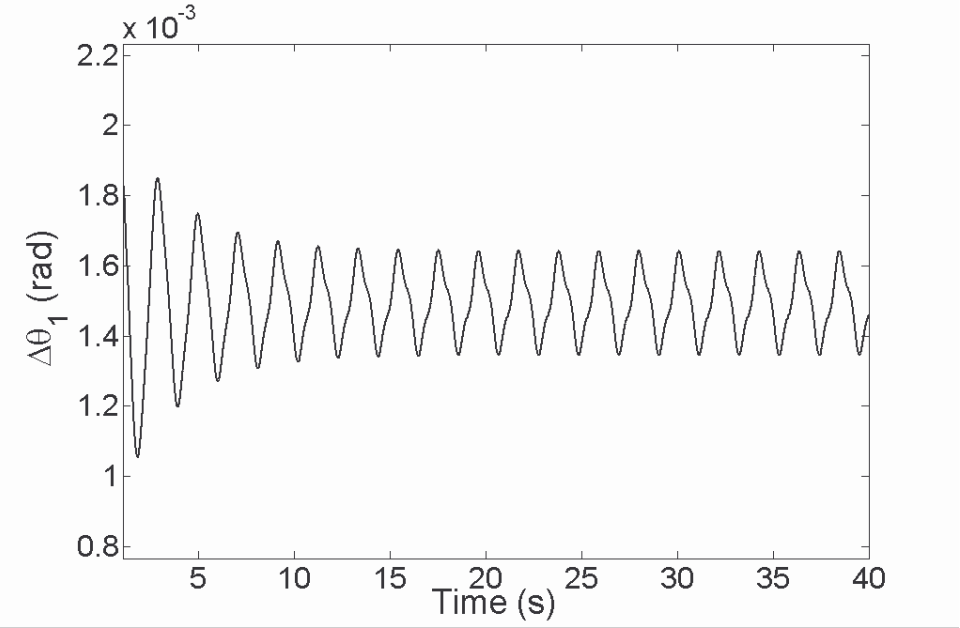

Figure **2.6**: Plot of the relative error in the angular displacements of the tail link between the explicit and implicit models for a three-link snake robot

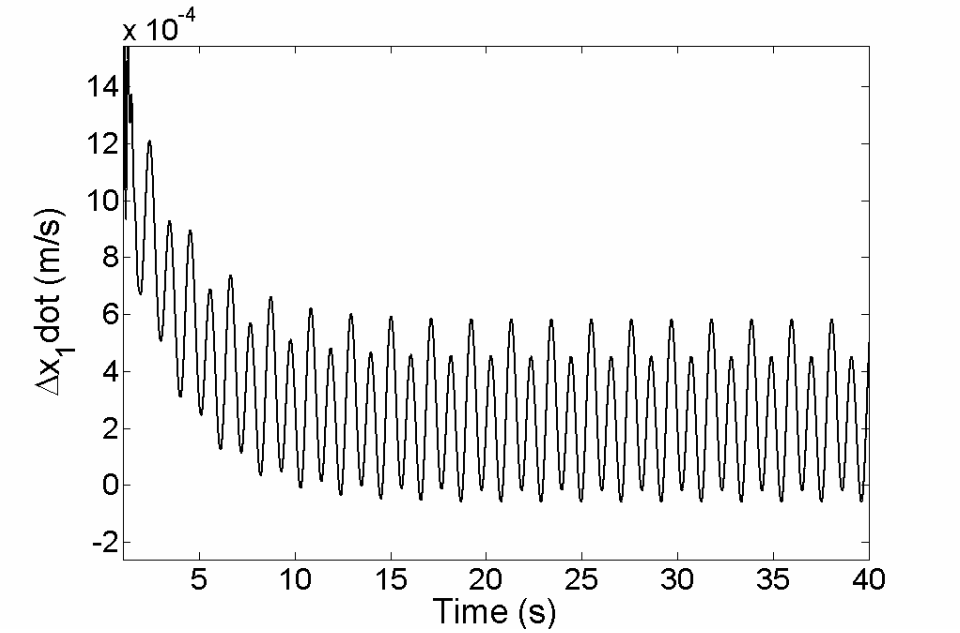

Figure **2.7**: Plot of the relative error in the forward velocities of the tail link between the explicit and implicit models for a three-link snake robot

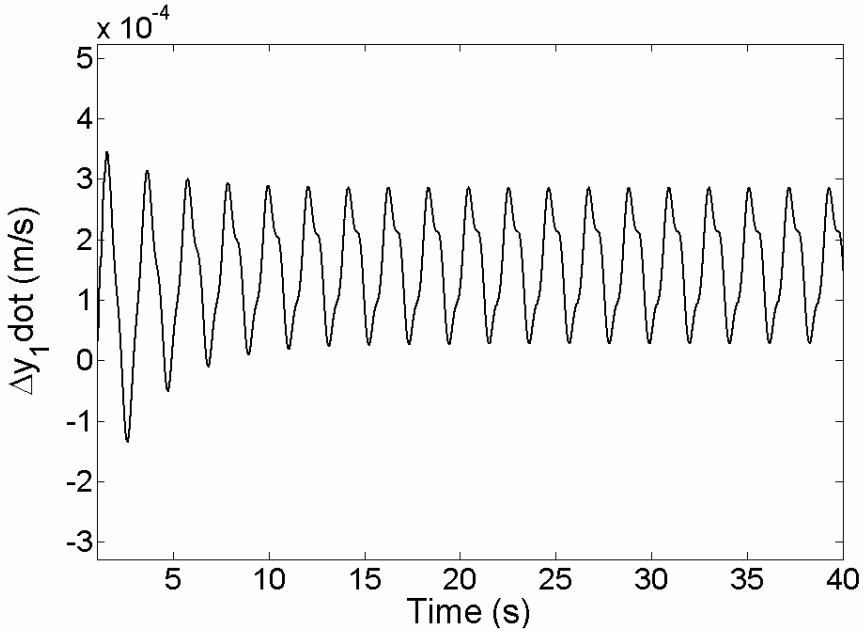

Figure **2.8**: Plot of the relative error in the transverse velocities of the tail link between the explicit and implicit models for a three-link snake robot

Chapter 3

OPTIMALLY EFFICIENT SERPENTINE LOCOMOTION

Having confirmed that the implicit method predicts locomotion behavior equally as well as an explicit model for a simple three-link robot, the implicit model is now used to analyze a six-link robot. Specifically, locomotion dynamics are studied to determine the optimal gait that minimizes the input energy (i.e. input power integrated over a given time) while maximizing the kinetic energy of forward locomotion. Earlier research [4] indicates that the undulatory motion of snake can be replicated by sending a traveling sine wave along the length of the snake. This wave can be approximated in a discrete snake model by incrementing the phase angle of applied torque or prescribed angular motion at each joint of the snake robot. This analysis considers the input to be a commanded joint angle with the angular motion at i^{th} joint described by the form:

$$\theta_i(t) = \alpha \sin(\omega t + \beta_i) \tag{3.1}$$

where, $\beta_i = (i-1)\beta$ and $i = 1, 2, \ldots n-1$

The parameter ω (frequency of sine wave input) is related to the speed of locomotion, while the parameters α (amplitude of angular displacement input) and β (relative phase lag) are related to the shape of forward motion. A trace of the path followed by the snake robot at α = 30 deg, β = 80 deg and ω = 5 rads^{-1} and C_t = 0.1 and C_n = 10 is presented in Fig. 3.1 and a plot of the snake's position and orientation at six instances over one time period is shown in Fig. 3.2. Performance index, η, is defined as

the ratio of kinetic energy of forward locomotion to input energy over one time period. The optimally efficient motion is defined as the set of parameters - α and β that maximize the performance index for a given frequency ω and friction characteristics. The input energy, denoted by *IE*, is calculated by integrating the power input over one time period. Equivalently, input energy is defined as: $P_{in} \cdot T$; where, P_{in} is the mean power input and $T = \frac{2\pi}{\omega}$ is the time period. The power input is defined as the sum of the products of joint torques and corresponding relative angular velocities at all the joints. A plot of the variation of power input with time for α = 30 deg, β = 80 deg and ω = 5 rads^{-1} is shown in Fig. **3.3**. The mean power input is determined by averaging the periodic input power over 14 time periods from *T* to 15**T*. The kinetic energy of forward locomotion, *KE*, is defined as: $\frac{1}{2}mv^2$ where, *v* is the mean forward velocity of the center of mass of the snake in the global x-direction averaged over 14 time periods as indicated earlier.

An effective method for analyzing the optimally efficient locomotion is to utilize the dimensional analysis and Buckingham's pi theorem [**26**] to combine the various parameters influencing the snake's locomotion into a group of dimensionless parameters. This helps in reducing the computational difficulties associated with the wide range of parameter search in the dimensional domain. The following sections will concentrate upon the introduction of dimensional analysis and Buckingham's pi theorem and their application in the analysis of non-dimensional parameter space to determine the optimal gait of the snake robot.

3.1 Dimensional Analysis

In many applications of science and engineering, the mathematical relationships between variables in a system are unknown. In order to find the relationship between these variables, one would require to incrementally change the value of one variable while holding all of the other variables constant. This process would then be repeated for each variable until the relationships were discovered. This would be a difficult and sometimes impossible procedure to perform. By combining the terms to reduce the number of variables, the process becomes less complicated and more reasonable to perform. Furthermore, the number of variables influencing the system's characteristics is also reduced; thus making it easy to analyze the overall system. This is achieved by performing a dimensional analysis on the set of parameters involved in a given physical problem.

Dimensional analysis is a mathematical technique where the parameters considered being likely to affect the flow can be combined into a number of dimensionless groups. If it is possible to identify the factors involved in a physical situation, dimensional analysis can usually establish the form of relationship between them. In dimensional analysis, one is concerned only with the nature of factors involved in the situation and not with their numerical values. This process of dimensional analysis is based on the Buckingham's pi theorem explained in the following section.

3.2 Buckingham pi theorem

The Buckingham pi theorem states that for a physically meaningful equation involving a certain number (N) of physical variables, where these N variables are expressible in terms of k independent fundamental physical quantities, the original expression is equivalent to an equation involving a set of $p = N - k$ dimensionless variables constructed from the original variables. These dimensionless variables are often referred to as π parameters. Thus the number of π variables required to describe a system is k less than the original number of variables. The k repeating (independent) variables that will be combined with each remaining variable to form the π parameters must include all the basic dimensions, but should not form a π-parameter by themselves. Consider a physically meaningful equation such as:

$$f(q_1, q_2, \ldots, q_n) = 0 \tag{3.2}$$

where, $q_i, (i = 1, 2, \ldots, n)$ are the N physical variables, which are expressed in terms of k independent physical units, then the above equation can be rewritten as:

$$F(\pi_1, \pi_2, \ldots, \pi_p) = 0 \tag{3.3}$$

where, the π_i's are p dimensionless parameters constructed from the q_i's and are represented by equations of the form:

$$\pi_i = q_i \cdot (q_{p+1})^{m_1{}^i} \cdot (q_{p+2})^{m_2{}^i} \cdot \ldots \cdot (q_n)^{m_k{}^i} \tag{3.4}$$

where $i = 1, 2, \ldots, p$; $q_{p+1} - q_n$ are k independent physical quantities and the exponents m_j^i's $(j = 1, 2, \ldots, k)$ are constants and are determined subject to the dimensional homogeneity criterion i.e. all π_i's should necessarily be non-dimensional.

The Buckingham pi theorem provides a method for computing sets of dimensionless parameters from the given variables, even if the form of the equation is unknown. However, the choice of dimensionless parameters is not unique. However, one must choose a set of parameters that tend to simplify the analysis as much as possible. The application of pi theorem to analyze the optimally efficient serpentine locomotion is detailed below.

In order to perform dimensional analysis, one must first list all of the variables that define a problem, including dimensional and non-dimensional quantities. For a snake robot, the physical variables governing the dynamics are – n, m, l, α, β, ω, C_t, C_n, P_{in}, v, T, k, c, dt, K_p and K_d. The last three parameters not listed in the analysis earlier are defined as follows:

dt Fixed time step used in simulation

K_p Proportional gain

K_d Derivative gain

An equation similar to Eq. (**3.2**), involving these N (= 16) physical variables can be written as:

$$f\left(n, m, l, \alpha, \beta, \omega, C_t, C_n, P_{in}, v, T, k, c, dt, K_p, K_d\right) = 0 \qquad (\mathbf{3.5})$$

The dimensions of these variables are:

$[n]$	=	[Number (of links)]	=	[1]	
$[m]$	=	[Mass (of link)]	=	[M]	
$[l]$	=	[Length (of link)]	=	[L]	
$[\alpha]$	=	[Angle (amplitude), radians]	=	[1]	
$[\beta]$	=	[Angle (phase), radians]	=	[1]	
$[\omega]$	=	[Frequency]	=	$[T^{-1}]$	
$[C_t]$	=	[Viscous friction coefficient (tangential direction)]	=	$[MT^{-1}]$	
$[C_n]$	=	[Viscous friction coefficient (normal direction)]	=	$[MT^{-1}]$	
$[P_{in}]$	=	[Power]	=	$[ML^2T^{-3}]$	(**3.6**)
$[v]$	=	[Velocity]	=	$[LT^{-1}]$	
$[T]$	=	[Time]	=	[T]	
$[k]$	=	[Spring stiffness]	=	$[MT^{-2}]$	
$[c]$	=	[Damping constant]	=	$[MT^{-1}]$	
$[dt]$	=	[Time]	=	[T]	
$[K_p]$	=	[Angular displacement to torque proportional gain]	=	$[ML^2T^{-2}]$	
$[K_d]$	=	[Angular displacement to torque derivative gain]	=	$[ML^2T^{-1}]$	

The number of fundamental dimensions in the above set of variables is: $k = 3$ (M, L, and T) and the number of dimensionless parameters is $p = n - k = 13$. Thus, three independent physical quantities have to be chosen such that they include the three aforementioned basic dimensions – M, L and T. Let the independent quantities be: m, l, and ω. A procedure to determine the non-dimensional quantity associated with the power input, π_1 is detailed as follows:

Since P_{in} contains all the three fundamental dimensions M, L and T, all three of the repeating variables will feature in the corresponding dimensionless group. Expressing π_1 as:

$$\pi_1 = Pm^a l^b \omega^c \tag{3.7}$$

and replacing the variables by their corresponding dimensions, yields:

$$[M^0L^0T^0]=[ML^2T^{-3}][M]^a[L]^b[T^{-1}]^c \quad (3.8)$$

Comparing the powers of M, L and T, on either side results in:

$$\begin{aligned} 0 &= 1 + a \\ 0 &= 2 + b \\ 0 &= -3 - c \end{aligned} \quad (3.9)$$

The above set of simple equations can be solved to obtain the values of the indices as: a = -1, b = -2 and c = -3. The π parameter associated with the power input is therefore expressed as: $\pi_1 = \frac{P_{in}}{ml^2\omega^3}$. The above process is repeated for the remaining variables and the thirteen π parameters are found to be as follows:

$$
\begin{aligned}
\pi_1 &= \frac{P_{in}}{ml^2\omega^3} \\
\pi_2 &= \frac{v}{l\omega} \\
\pi_3 &= \alpha \\
\pi_4 &= \beta \\
\pi_5 &= \frac{C_t}{m\omega} \\
\pi_6 &= \frac{C_n}{m\omega} \\
\pi_7 &= T \cdot \omega \\
\pi_8 &= \frac{k}{m\omega^2} \\
\pi_9 &= \frac{c}{m\omega} \\
\pi_{10} &= dt \cdot \omega \\
\pi_{11} &= \frac{K_p}{ml^2\omega^2} \\
\pi_{12} &= \frac{K_d}{ml^2\omega} \\
\pi_{13} &= n
\end{aligned}
\tag{3.10}
$$

Since π_1 and π_2 (i.e. outputs) are dependent on π_3, π_4, …, π_{13} (inputs); as long as these eleven input π parameters are held constant, the dependent parameters will remain the same. Hence the fundamental physical quantities, m, l and ω do not influence the dimensionless outputs π_1 and π_2, and any other output π parameter (e.g. dimensionless kinetic energy or input energy) as long as the input π parameters are held constant. It is to be noted that π_8, π_9, π_{11} and π_{12} do not directly influence the outputs, but are needed to meet the compatibility conditions.

3.3 Optimal Gait Analysis

As defined earlier, optimally efficient motion is the set of parameters - α and β that maximize the ratio of kinetic energy to input energy (ratio denoted as η) at a given frequency, ω. Other design parameters also affect the optimal motion; these include the tangential and normal friction coefficients, the mass and length of the link, and the number of links. But these input parameters namely; friction coefficients, number of links, etc. (except α and β) are fixed in the design of the snake and cannot be modified by the input to the joints, e.g. the snake's control algorithm. Since the analysis is performed in the dimensionless space and m, l and ω are the base variables, these do not have any bearing on the optimal solution as stated earlier. This attribute of the dimensional analysis is useful in experimental analysis, where changes in mass or length of the link do not change the predicted optimal gait and the optimal parameters do not have to be rederived.

To determine the optimally efficient gait, one can use either a mathematical solution or an iterative search. In this study, both the solution methods are considered. To begin with, a search through a range of the parameters α and β is undertaken to determine the existence of optimal gait parameters. This is necessary to establish the uniqueness of the optimal solution. The performance index, η can be expressed as:

$$\eta = \frac{KE}{IE} = \frac{\frac{1}{2}mv^2}{P_{in} \cdot T} \tag{3.11}$$

Eq. (3.11) can be rearranged to obtain the following:

$$\eta = \frac{1}{2} \frac{\left(\frac{v}{L\omega} \right)^2}{\left(\frac{P}{mL^2\omega^3} \right)} \cdot \frac{1}{T\omega} \tag{3.12}$$

Furthermore, the above equation can be rewritten using the dimensionless groups derived in Eq. (**3.10**) as follows:

$$\eta = \frac{1}{2} \frac{\pi_2}{\pi_1 \pi_7} \tag{3.13}$$

which can be considered as another output besides π_1 and π_2 and hence, will satisfy all the properties that hold true for π_1 and π_2.

A plot of the performance index, η as a function of α and β is shown in Fig. **3.4** and projections of the plot onto the $\alpha - \eta$ and $\beta - \eta$ planes are shown in Figs. **3.5** and **3.6** respectively. A contour plot illustrating the variation of η with α and β is shown in Fig. **3.7**. An enlarged version of the same plot around the optimal value (the blue dot) is presented in Fig. **3.8**. These plots indicate that an optimum exists and that it is unique. The maximum performance index, $\eta_{\max}$ predicted by the iterative search technique for $\pi_5 = 0.1$, $\pi_6 = 10.0$ is approximately 0.106. The corresponding values of optimal phase β_{opt} and optimal amplitude α_{opt} predicted are 85 deg and 34 deg respectively. From Fig. **3.8**, the variation of $\eta_{\max}$ around $\alpha = \alpha_{opt} \pm 5$ deg and $\beta = \beta_{opt} \pm 5$ deg is approximately 1%. This indicates that the maximum performance index is fairly robust to minor variations in the optimal parameters.

It is however numerically challenging to determine these optimal parameters using the iterative search because of the enormous amount of time and effort required, the

lack of efficiency and accuracy of the predicted optimal solution. A non-linear optimization routine is therefore used to overcome these difficulties associated with the iterative search technique and simplify the solution process.

Matlab multi-variable optimization search routine - *fminsearch* is used to estimate the maxima. Since *fminsearch* can only find the minimum of a function, the variables that maximize η (i.e. α and β) are equivalently obtained by searching for the minimum of ($-\eta$). Table **3.1** represents the variation of optimal parameters as a function of the frequency maintaining the non-dimensional friction coefficients constant at $\pi_5 = 0.1$ and $\pi_6 = 10$. It can be seen that there is no variation in the optimal parameters with ω, as suggested by the Buckingham pi theorem. So for a given set of dimensionless friction coefficients, the optimal parameter search can be done at any frequency as long as the dimensionless inputs are kept constant. This methodology is hereafter used to determine the optimal parameters of the snake robot operating at a frequency of 5 rads^{-1}.

The variation of optimal parameters with dimensionless friction coefficients, $\pi_5 = \frac{C_t}{m\omega}$ and $\pi_6 = \frac{C_n}{m\omega}$ while maintaining the friction ratio - $\frac{\pi_6}{\pi_5} = \frac{C_n}{C_t}$ constant at 10 is presented in Table **3.2**. This ratio is characteristic of the snake operating on a treadmill and further description of this friction model is presented in Chapter 4. A plot of the variation of $\eta_{\max}$ with π_5 is shown in Fig. **3.9**. The maximum performance index decreases with the non-dimensional tangential friction coefficient as seen in the plot. A plot of the variation of corresponding optimal values of amplitude and relative phase angle is presented in Fig. **3.10** and a plot of the variation of non-dimensional velocity and

power is shown in Fig. **3.11**. The following conclusions can be drawn from the above plots:

- The variation of optimal amplitude and phase with the friction coefficient is relatively small for values of $\pi_5 < 10$. This indicates that for a given friction ratio, the dependence of optimal parameters upon the actual tangential friction ratio is minimal.
- The dimensionless forward locomotion velocity initially increases with increase in tangential friction coefficient but then decreases for higher values of π_5. The non-dimensional power input seems to increase steadily with π_5. As indicated earlier, $\eta_{\max}$ decreases approximately by an order of magnitude with an order of magnitude increase in the tangential friction coefficient.
- For a given frequency, as π_5 increases, the tangential friction coefficient increases. For the snake to translate forward at approximately the same velocity, the power consumption has to increase with increase in tangential friction coefficient; which is confirmed by the results plotted in Fig. **3.11** and in Table **3.2**.
- The drop in velocity at higher values of π_5 can be attributed to the fact that more energy is expended in overcoming the friction in forward direction and not as much is converted into kinetic energy

In addition to determining the variation of optimal parameters with dimensionless friction coefficients for a friction ratio of 10, the variation for other friction ratios can also be studied. Tables **3.3** and **3.4** show the variation of the optimal parameters for friction ratios of 100 and 1000 respectively. The variations of α_{opt} between Tabs. **3.2** - **3.4** for

various friction ratios is plotted in a single graph and is shown in Fig. **3.12**. Similarly, the variations of other optimal parameters are shown in Figs. **3.13** - **3.16**.

Furthermore, the variation of $\eta_{\max}$ is studied maintaining π_5 constant at 1, a value characteristic of the snake robot operating on the treadmill and varying the ratio of friction coefficients $\frac{C_n}{C_t}$ and the results are tabulated in Tab. **3.5**. A plot of the variation of $\eta_{\max}$ with the friction ratio is shown in Fig. **3.17**. A plot of the variation of corresponding α_{opt} and β_{opt} is presented in Fig. **3.18** and a plot of the variation of the outputs π_1 and π_2 is shown in Fig. **3.19**. The following conclusions can be drawn from these plots in conjunction with Figs. **3.12** - **3.16**:

- At $\pi_5 = 1$ (Fig. **3.17**), the maximum performance index increases with increase in friction ratio. This indicates that for a given tangential friction coefficient, as the normal coefficient increases, $\eta_{\max}$ increases. This is expected because, at higher values of normal friction coefficient, the snake is not as much prone to move sideways as it is at lower normal friction coefficients. However, the change in $\eta_{\max}$ with friction ratio is not as high as compared to the change in $\eta_{\max}$ with the actual tangential friction coefficient (see Fig. **3.14**).
- From Fig. **3.18**, at $\pi_5 = 1$ and for friction ratios less than 100, α_{opt} seems to decrease exponentially with friction ratio, but β_{opt} seems to be approximately constant. However, at higher values of π_5 and friction ratio, i.e. higher values of

tangential and normal friction coefficients, there seems to be a sudden increase in β_{opt}. This trend is also confirmed by Fig. **3.13**.

- The velocity at $\pi_5 = 1$, appears to increase with increase in friction ratio(Fig. **3.19**), but seems to decrease as the ratio is increased beyond 100. However, for values of $\pi_5 < 0.1$ (Fig. **3.16**), the optimal velocity increases steadily with increase in the friction ratio. The variation of power does not exhibit any particular trend, but similar to $\eta_{\max}$, the variation with friction ratio is not as predominant as the variation with tangential friction coefficient.

Compared to an earlier study [**19**], the results of the present research match qualitatively but not quantitatively. For instance, the present study predicts that an optimal motion for a friction ratio of 100 and $1 < \pi_5 < 0.02$ should consist of slightly more than one full sine wave (1.4 sine waves), while this earlier study predicted optimal motion for exactly one sine wave. This is equivalently described by comparing the optimal phase, β_{opt} of a six-link robot. The present study predicts β_{opt} to be at approximately 85 deg between links, while [**19**] predicts this to be at 60 deg. The variation of optimal amplitude α_{opt} predicted by [**19**] seems to be roughly linear with desired velocity, while the present study predicts a nearly constant value at 34 deg. The optimal frequency of serpentine motion, ω_{opt}, is predicted by the present study to vary linearly with the desired velocity in agreement with this prior work.

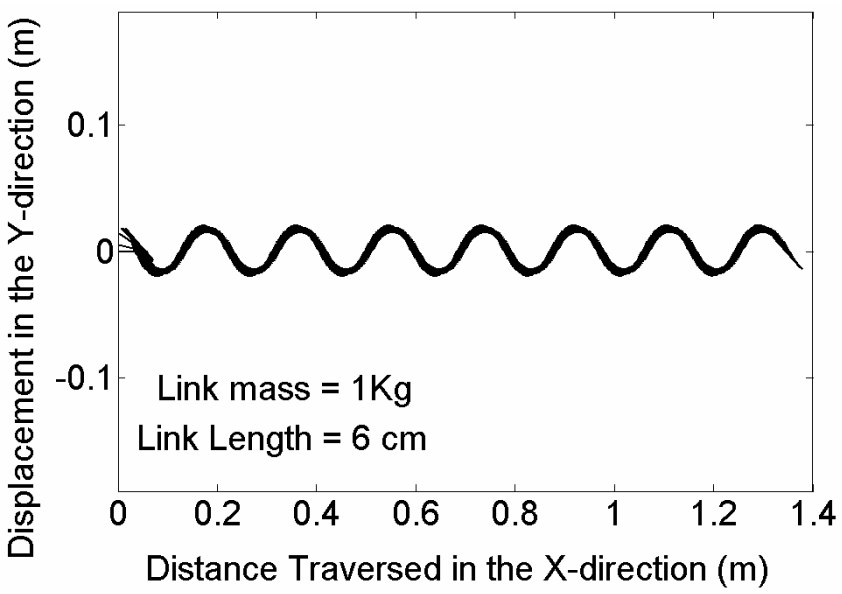

Figure **3.1**: Trace of the path followed by the snake robot over a time of 9 s at α = 30 deg β = 80 deg and ω = 5 rads^{-1}

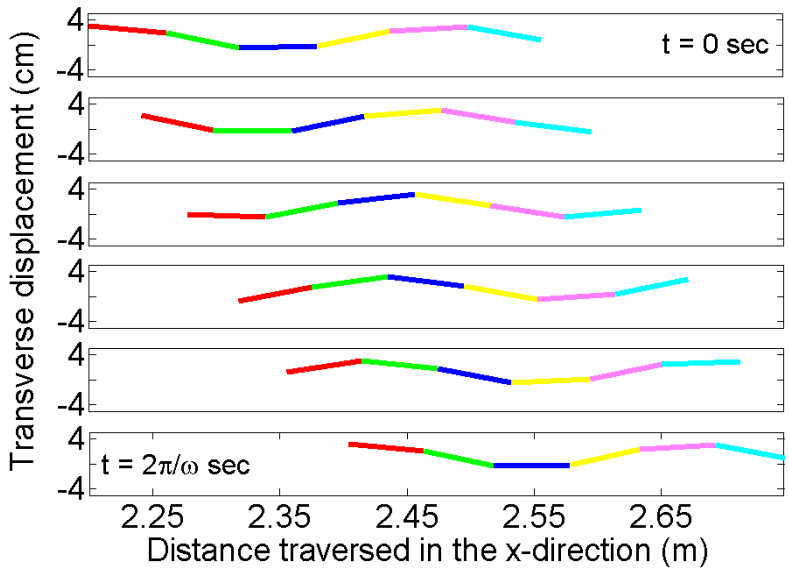

Figure **3.2**: Plot of the snake's position at six instances over one time period at α = 30 deg, β = 80 deg, and ω = 5 rads^{-1}

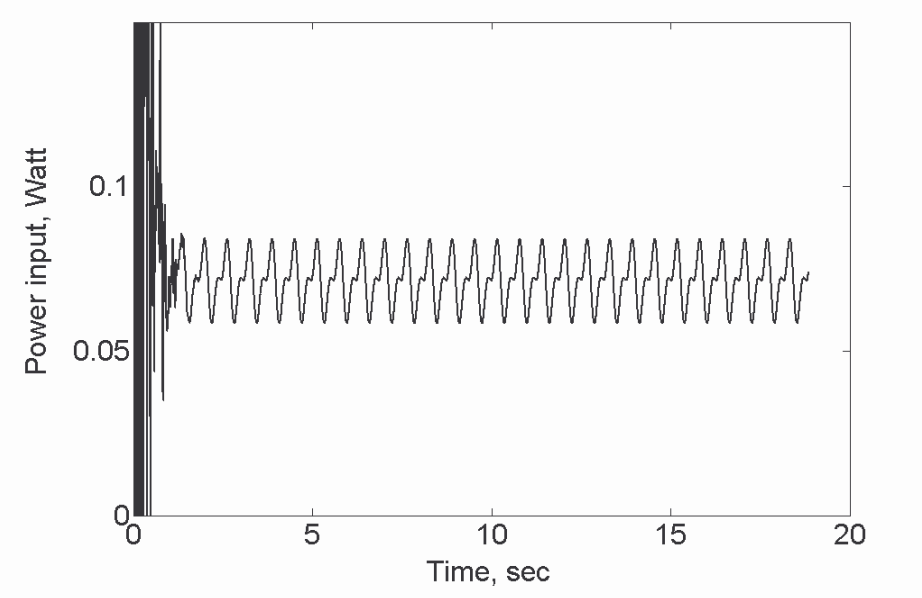

Figure **3.3**:Variation of power input over 15 cycles for α = 30 deg, β = 80 deg and ω = 5 rads^{-1}

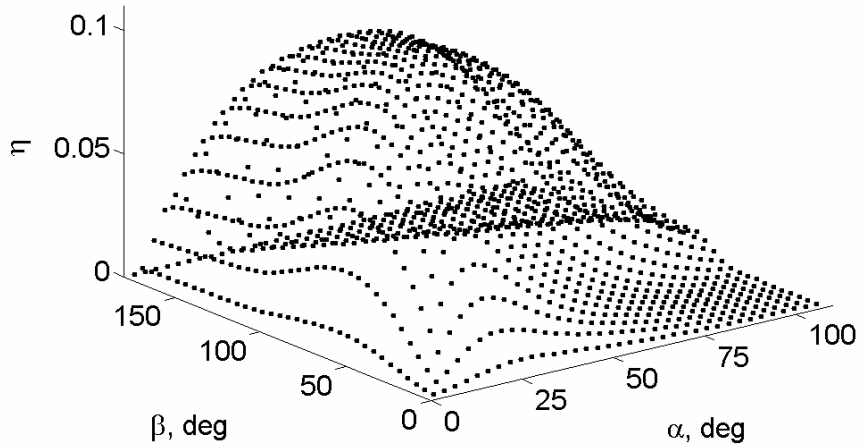

Figure **3.4**: Plot of the performance index, η as a function of amplitude, α and relative phase angle, β indicating the presence of an unique optimum

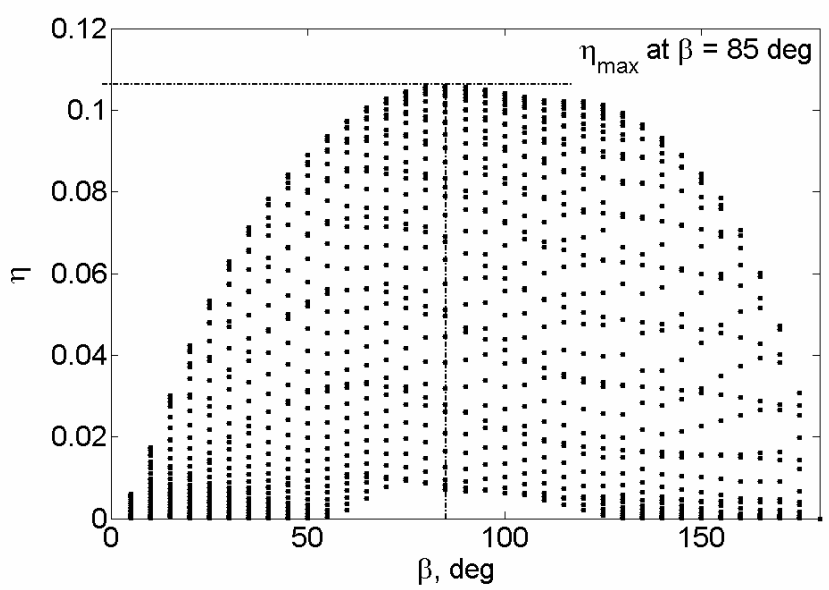

Figure **3.5**: Plot of the performance index, η as a function of relative phase angle, β indicating the occurrence of maximum at $\beta \approx 34$ deg

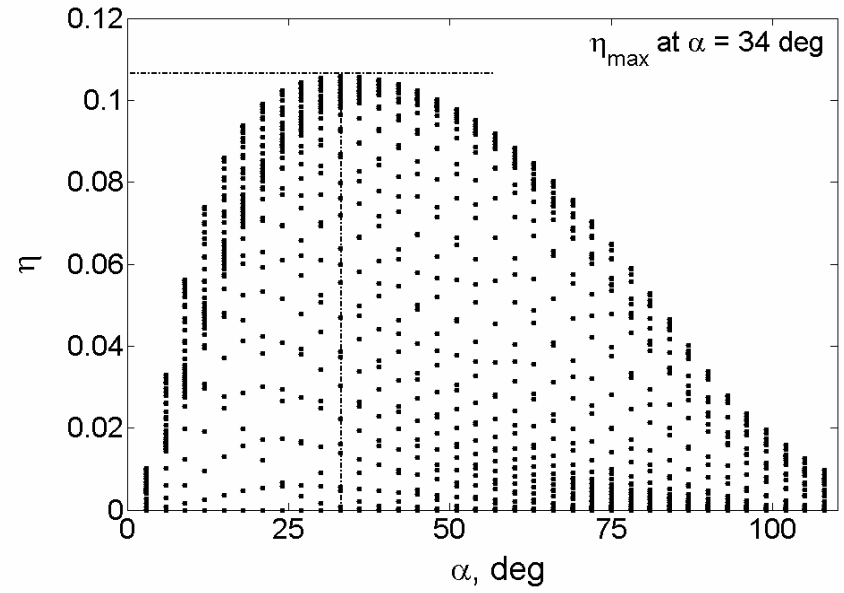

Figure **3.6**: Plot of the performance index, η as a function of amplitude, α indicating the occurrence of maximum at $\alpha \approx 34$ deg

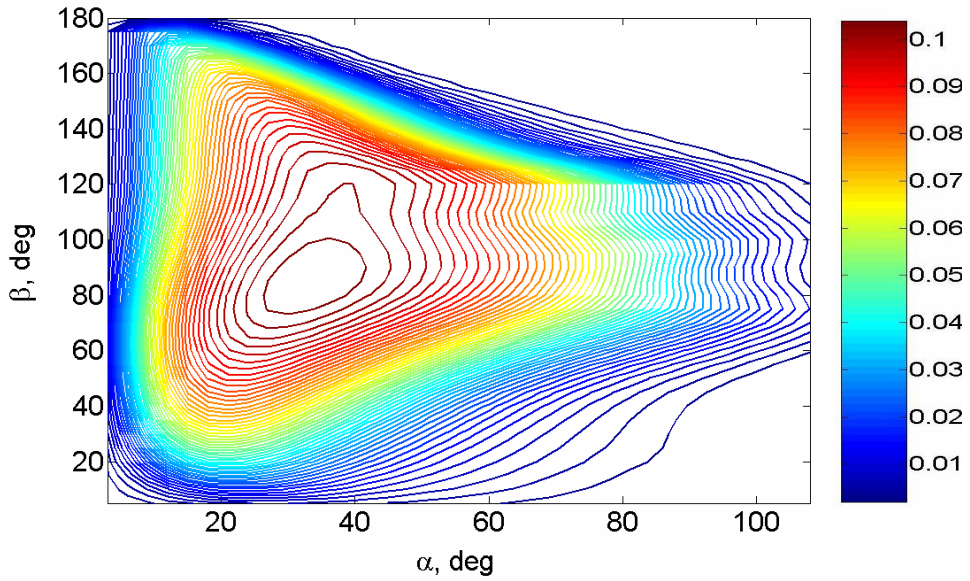

Figure **3.7**: Contour plot showing the variation of performance index, η as a function of amplitude, α and relative phase angle, β

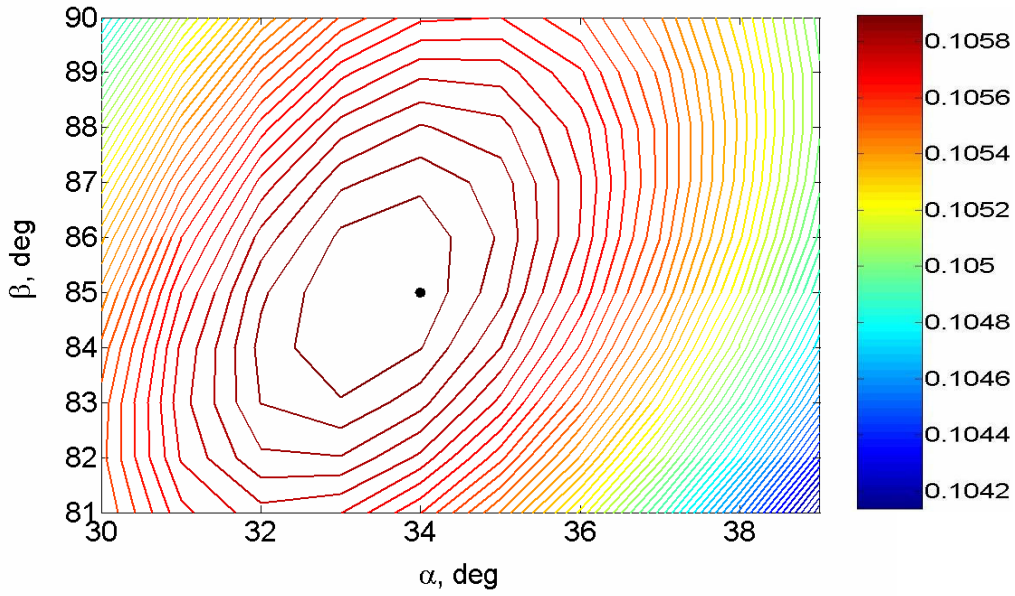

Figure **3.8**: Contour plot around the optimal value depicting the robustness of the predicted solution

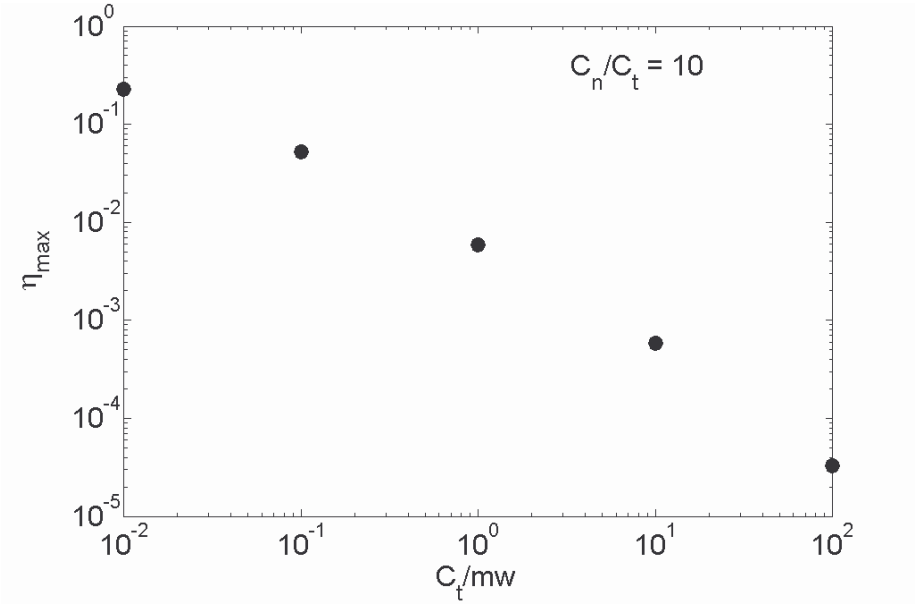

Figure **3.9**: Plot of the variation of maximum performance index with dimensionless tangential friction coefficient maintaining the friction ratio at 10

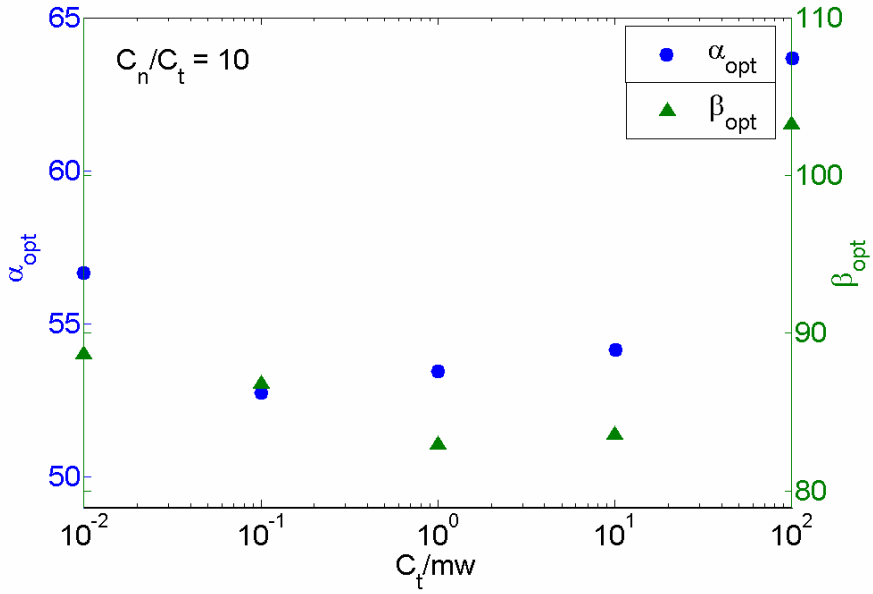

Figure **3.10**: Plot of the variation of α_{opt} and β_{opt} with dimensionless tangential friction coefficient maintaining the friction ratio at 10

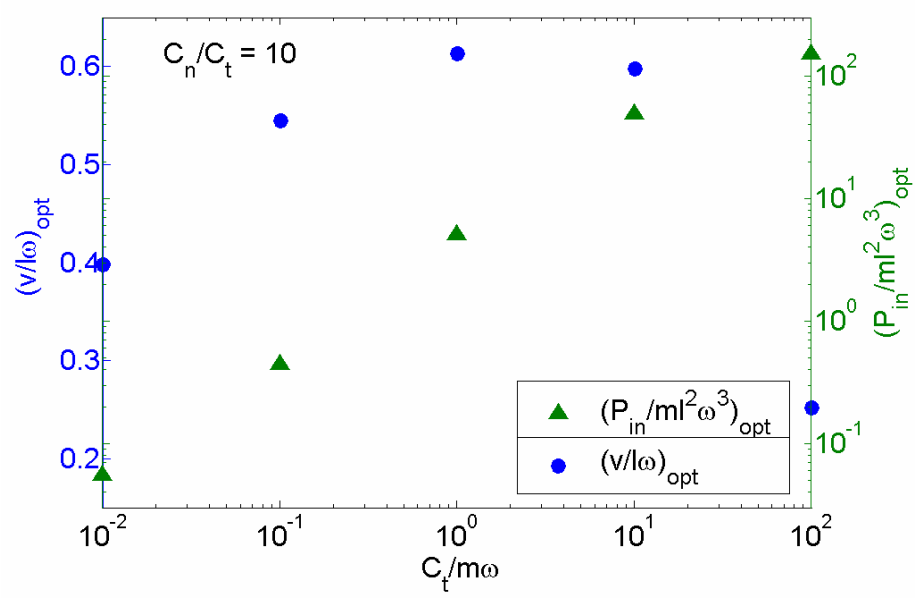

Figure **3.11**: Plot of the variation of dimensionless power and velocity with dimensionless tangential friction coefficient maintaining the friction ratio at 10

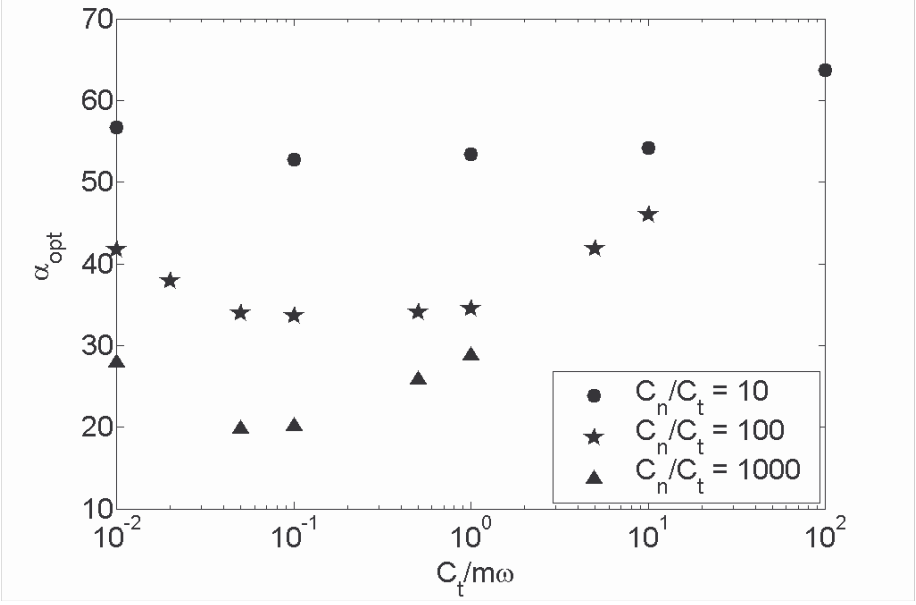

Figure **3.12**:Plot of the variation of α_{opt} with dimensionless tangential friction coefficient for various friction ratios

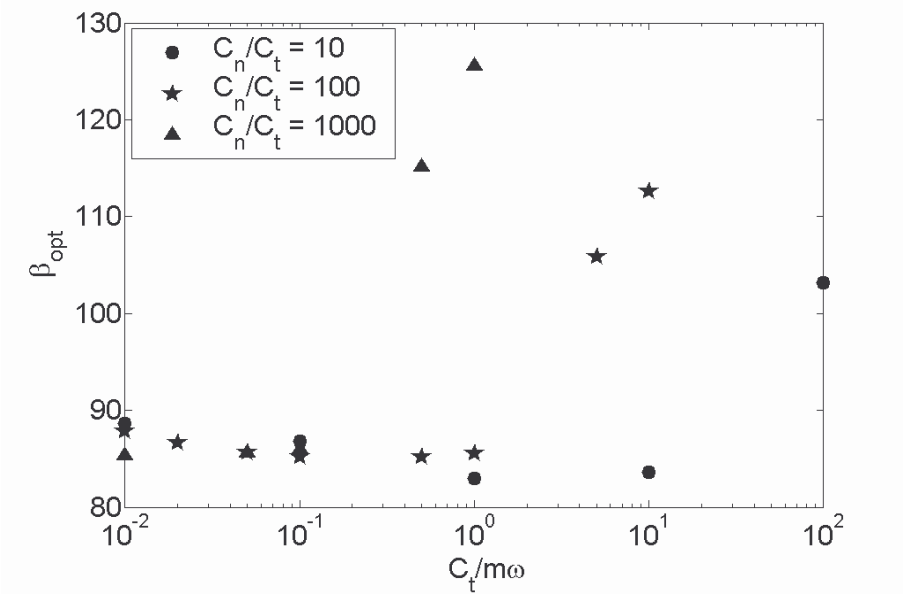

Figure **3.13**: Plot of the variation of β_{opt} with dimensionless tangential friction coefficient for various friction ratios

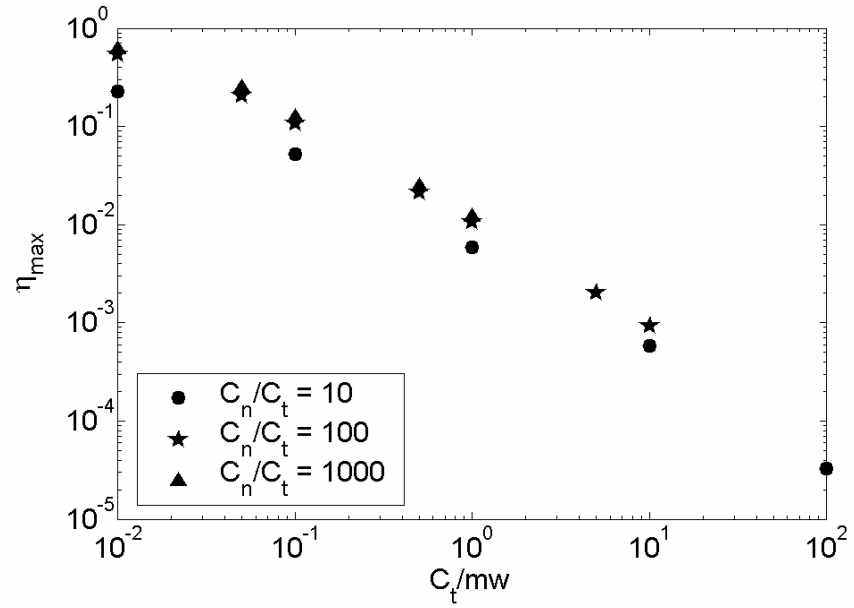

Figure **3.14**: Plot of the variation of $\eta_{\max}$ with dimensionless tangential friction coefficient for various friction ratios

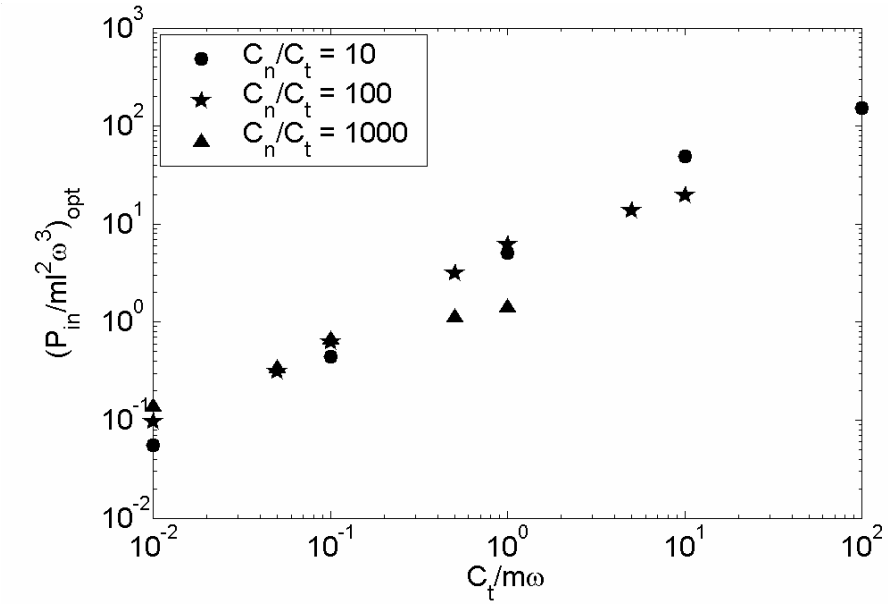

Figure **3.15**: Plot of the variation of dimensionless power with dimensionless tangential friction coefficient for various friction ratios

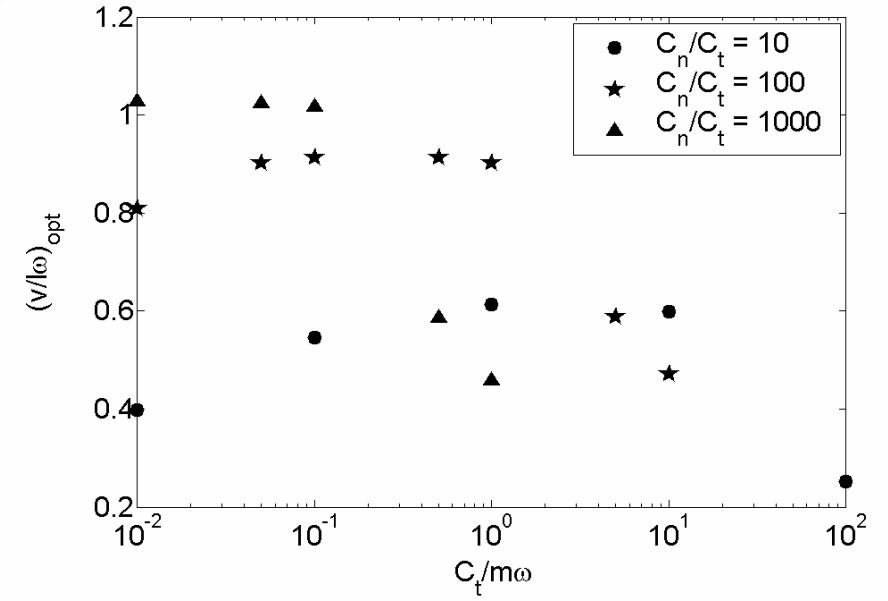

Figure **3.16**: Plot of the variation of dimensionless velocity with dimensionless tangential friction coefficient for various friction ratios

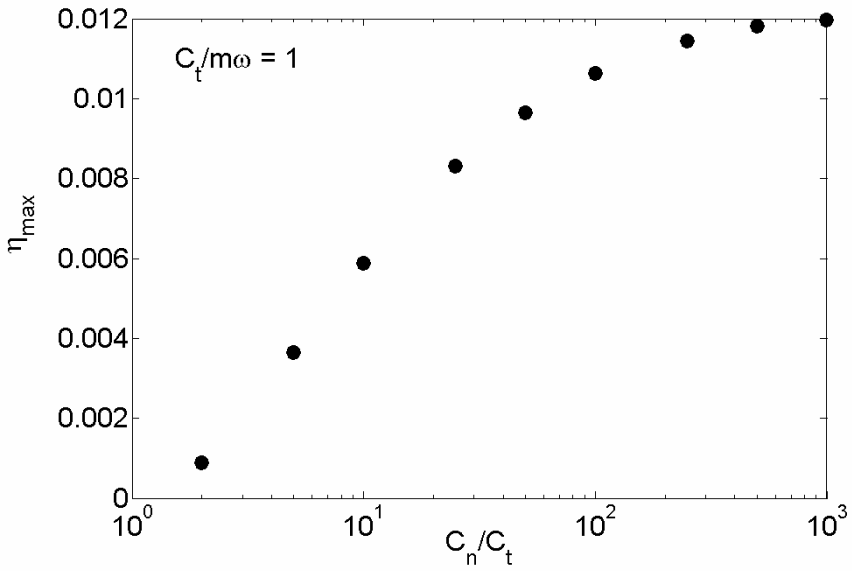

Figure **3.17**: Plot of the variation of maximum performance index with the friction ratio maintaining the dimensionless tangential friction coefficient at 1

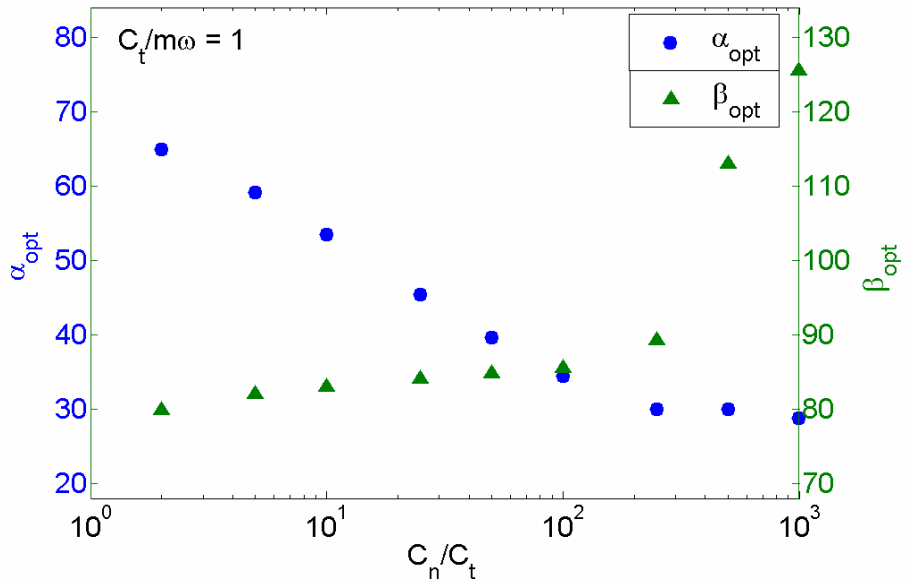

Figure **3.18**: Plot of the variation of α_{opt} and β_{opt} with the friction ratio maintaining the dimensionless tangential friction coefficient at 1

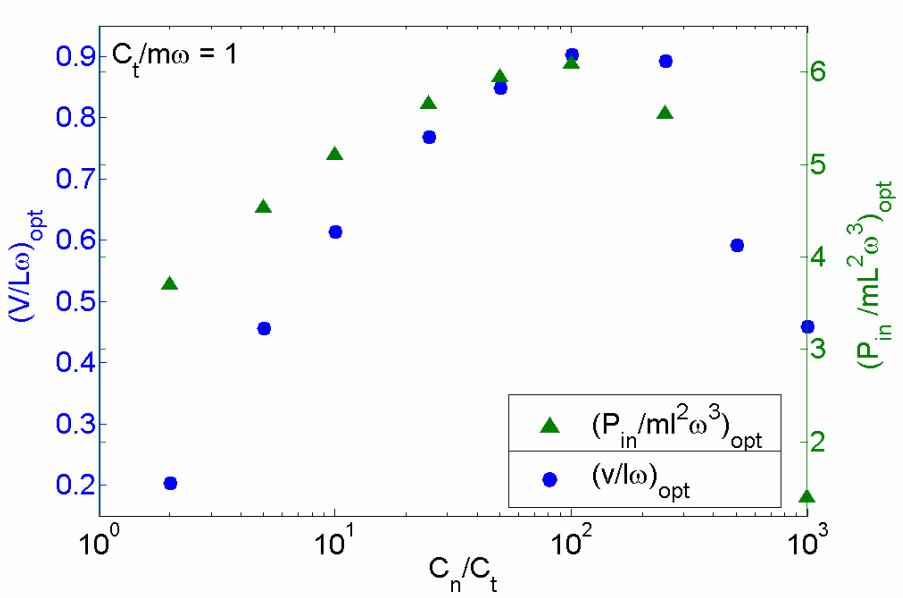

Figure **3.19**: Plot of the variation of dimensionless power and velocity with the friction ratio maintaining the dimensionless tangential friction coefficient at 1

Table **3.1**: Variation of the optimal parameters as a function of ω while maintaining the non-dimensional friction coefficients constant at $\pi_5 = 0.1$ and $\pi_6 = 10.0$

α_{opt} (deg)	β_{opt} (deg)	ω ($rads^{-1}$)	$\eta_{\max}$	$\pi_2 = \frac{v}{l\omega}$	$\pi_1 = \frac{P_{in}}{ml^2\omega^3}$
33.561	85.144	1	$1.061*10^{-1}$	0.912	0.624
33.561	85.144	2	$1.061*10^{-1}$	0.912	0.624
33.561	85.144	3	$1.061*10^{-1}$	0.912	0.624
33.561	85.144	4	$1.061*10^{-1}$	0.912	0.624
33.561	85.144	5	$1.061*10^{-1}$	0.912	0.624
33.561	85.144	6	$1.061*10^{-1}$	0.912	0.624
33.561	85.144	10	$1.061*10^{-1}$	0.912	0.624
33.561	85.144	15	$1.061*10^{-1}$	0.912	0.624
33.561	85.144	20	$1.061*10^{-1}$	0.912	0.624
33.561	85.144	25	$1.061*10^{-1}$	0.912	0.624

Table **3.2**:Variation of the optimal parameters with dimensionless friction coefficients, π_5 and π_6 while maintaining the friction ratio $\frac{\pi_6}{\pi_5}$ constant at 10

π_5	α_{opt} (deg)	β_{opt} (deg)	$\eta_{\max}$	$\pi_2 = \frac{v}{l\omega}$	$\pi_1 = \frac{P_{in}}{ml^2\omega^3}$
0.01	56.669	88.646	$2.278*10^{-1}$	0.397	0.055
0.10	52.755	86.786	$5.261*10^{-2}$	0.546	0.448
1.00	53.447	82.965	$5.871*10^{-3}$	0.614	5.101
10.0	54.141	83.575	$5.874*10^{-4}$	0.598	49.168
100.0	63.658	103.210	$3.306*10^{-5}$	0.252	152.116

Table **3.3**: Variation of the optimal parameters with dimensionless friction coefficients, π_5 and π_6 while maintaining the friction ratio $\frac{\pi_6}{\pi_5}$ constant at 100

π_5	α_{opt} (deg)	β_{opt} (deg)	$\eta_{\max}$	$\pi_2 = \frac{v}{l\omega}$	$\pi_1 = \frac{P_{in}}{ml^2\omega^3}$
0.01	41.669	87.854	$5.399*10^{-1}$	0.808	0.096
0.05	33.923	85.588	$2.067*10^{-1}$	0.902	0.312
0.10	33.561	85.144	$1.061*10^{-1}$	0.912	0.624
0.50	34.079	85.122	$2.135*10^{-2}$	0.912	3.103
1.00	34.441	85.554	$1.064*10^{-2}$	0.902	6.088
5.00	41.826	105.83	$2.007*10^{-3}$	0.588	13.6704
10.0	45.985	112.590	$9.173*10^{-4}$	0.472	19.268

Table **3.4**: Variation of the optimal parameters with dimensionless friction coefficients, π_5 and π_6 while maintaining the friction ratio $\frac{\pi_6}{\pi_5}$ constant at 1000

π_5	α_{opt} (deg)	β_{opt} (deg)	$\eta_{\max}$	$\pi_2 = \frac{v}{l\omega}$	$\pi_1 = \frac{P_{in}}{ml^2\omega^3}$
0.01	22.111	85.447	$6.140*10^{-1}$	1.027	0.137
0.05	19.769	85.601	$2.483*10^{-1}$	1.024	0.336
0.10	20.087	85.946	$1.241*10^{-1}$	1.016	0.664
0.50	25.768	115.120	$2.447*10^{-2}$	0.586	1.116
1.00	28.725	125.540	$1.197*10^{-2}$	0.460	1.404

Table **3.5**: Variation of the optimal parameters with the ratio of friction coefficients, $\frac{\pi_6}{\pi_5}$ while maintaining the non-dimensional tangential friction component, π_5 constant at 1

$\frac{\pi_6}{\pi_5} = \frac{C_n}{C_t}$	α_{opt} (deg)	β_{opt} (deg)	$\eta_{\max}$	$\pi_2 = \frac{v}{l\omega}$	$\pi_1 = \frac{P_{in}}{ml^2\omega^3}$
2	64.915	79.887	$8.876*10^{-4}$	0.204	3.7
5	59.153	81.986	$3.637*10^{-3}$	0.456	4.536
10	53.462	82.968	$5.871*10^{-3}$	0.614	5.101
25	45.440	84.043	$8.300*10^{-3}$	0.768	5.652
50	39.622	84.751	$9.653*10^{-3}$	0.850	5.940
100	34.441	85.554	$1.064*10^{-2}$	0.902	6.088
250	30.031	89.306	$1.144*10^{-2}$	0.894	5.552
500	29.976	112.93	$1.180*10^{-2}$	0.592	2.356
1000	28.722	125.51	$1.197*10^{-2}$	0.460	1.404

Chapter 4

EXPERIMENTAL VALIDATION

To validate the analytical results, a snake robot which consists of six rigid wheeled members actuated by servos at the five joints has been built. The wheels have been chosen so that they have little slip in the lateral direction i.e. they are able to generate large friction coefficients in the normal direction and have relatively low friction coefficients in the tangential or forward direction. Thus the experimental conditions were designed to qualitatively match the assumed friction characteristics in the analytic formulation. A picture of the six link snake robot operating on treadmill can be seen in Fig. **4.1**. The mass of each link, m is 75.6 grams and the length of each link ($2*l$) is 7.6 cm. The friction characteristics are measured by utilizing the capability of the treadmill to tilt it to a desired angle of forward inclination (or tilt) (γ) and run at a desired velocity.

4.1 Friction Characteristics of Treadmill

To measure the tangential friction characteristics, the snake is set free perfectly straight on the treadmill i.e. relative angles between the links to be 180 deg. This is accomplished by setting all the servo angles at 90 deg. Initially, γ is set to a very small angle (2 deg in this case) and then increased steadily. The velocity of the treadmill is increased until the gravity of the snake almost balances the frictional forces on the snake. The above process is repeated in steps of 0.2 deg until a speed of 1 m/s is reached which

is approximately the physical limit of the snake. Knowing the mass of the snake, m, and the tilt angle, γ, the tangential friction force, F_t can be calculated using the following relationship:

$$F_t = m \cdot g \cdot \sin\gamma \tag{4.1}$$

where, g: acceleration due to gravity.

Figure 4.2 shows a plot of the tangential friction characteristics. Assuming the tangential friction force to vary linearly with the tangential velocity, the tangential friction characteristics are predicted to vary as:

$$F_t = 0.084 \cdot v_t + 0.14 \tag{4.2}$$

where, v_t is the velocity in tangential direction.

To estimate the friction characteristics in the normal direction, the links are slightly bent alternately with the relative angle between adjacent links slightly less than 180 deg (Fig. 4.3) (165 deg in this case ($=180-2\lambda$ by definition)). As in the earlier case, this is attained by setting the servo angles alternatively at $(90 \pm \lambda)$deg. The friction measurements are repeated as indicated above. The force equilibrium equation in the direction of treadmill velocity can be written as:

$$F_t \cdot \cos\lambda + F_n \cdot \sin\lambda = m \cdot g \cdot \sin\gamma \tag{4.3}$$

where, F_n is the friction force in the normal direction.

Assuming F_t known in Eq. (4.3), solving for F_n yields:

$$F_n = \frac{(m \cdot g \cdot \sin\gamma - F_t \cdot \cos\lambda)}{\sin\lambda} \tag{4.4}$$

A plot of the normal friction characteristics is shown in Fig. **4.4**. Again, assuming a linear variation of normal friction force with the normal velocity, the normal friction characteristics are predicted to vary as follows:

$$F_n = 1.2 \cdot v_n + 0.27 \qquad (4.5)$$

where, v_n is the velocity in normal direction.

Equations (**4.2**) and (**4.5**) indicate that the friction characteristics of a snake operating on a treadmill surface resemble that of a viscous friction model with an offset or in other words, a Bingham friction model and not purely viscous as assumed in the analysis of optimal gait in Chapter 3. The optimal gait parameters have to be derived considering the offset in the friction characteristics. The procedure is detailed in the following section.

4.2 Optimal gait parameters for a Coulomb plus viscous friction model

A simple Coulomb plus viscous friction model (Fig. **4.5**) is governed by the relationship: $F_{cv} = \text{sign}(v) \cdot c_0 + c \cdot v$, where the *signum* function, sign(v) is defined as:

$$\text{sign}(v) = \begin{cases} -1 & \text{when } v < 0 \\ 0 & \text{when } v = 0 \\ 1 & \text{when } v > 0 \end{cases} \qquad (4.6)$$

and c_0 is the Coulomb friction coefficient, c the viscous friction coefficient and F_{cv} the friction induced force at the point of contact. Considering the tangential and normal directions, there are four friction coefficients; C_{t_0}, C_{n_0}, C_t and C_n. In addition to the

thirteen π parameters established in Chapter 3 (Eq. (**3.10**)), two additional π parameters corresponding to the Coulomb friction coefficients, C_{t_0} and C_{n_0} are needed to complete the set of dimensionless parameters. These two π variables are expressed as:

$$\pi_{14} = \frac{C_{t_0}}{ml\omega^2}$$
$$\pi_{15} = \frac{C_{n_0}}{ml\omega^2} \qquad (4.7)$$

The variation of the optimal gait parameters under the influence of Coulomb plus viscous friction model is studied maintaining the tangential and normal viscous friction coefficients constant at $\pi_5 = 1.0$ and $\pi_6 = 10.0$. The dimensionless Coulomb friction coefficients $\frac{C_{t_0}}{ml\omega^2}$ and $\frac{C_{n_0}}{ml\omega^2}$ are varied around the experimentally determined nominal values of 2 and 4 respectively. Specifically, the optimal parameters are determined for π_{14} and π_{15} = 1, 2, 5, 10 and are presented in Tab. **4.1**. A plot of the variation of $\eta_{\max}$ with π_{14} and π_{15} is presented in Fig. **4.6**. It can be seen that for a given dimensionless tangential Coulomb friction coefficient, π_{14}, $\eta_{\max}$ in general increases with increase in dimensionless normal Coulomb friction coefficient, π_{15}. Also, for a given π_{15}, $\eta_{\max}$ decreases with increasing π_{14}. Overall $\eta_{\max}$ is in general less than the base value of 0.59 % at zero Coulomb friction in the tangential and normal directions.

A plot of the variation of optimal amplitude α_{opt} and optimal phase β_{opt} with π_{14} and π_{15} is shown in Figs. **4.7** and **4.8** respectively. Variations in α_{opt} and β_{opt} do not exhibit any particular trend except that β_{opt} for a given π_{14} and π_{15} is in general less than

the base value of 83 deg at zero Coulomb friction in the tangential and normal directions. Figure **4.9** represents the variation of optimal dimensionless velocity with π_{14} and π_{15}. In general for a given dimensionless tangential Coulomb friction coefficient, π_2 increases with increase in dimensionless normal Coulomb friction coefficient and for a given π_{15}, π_2 decreases with increase in π_{14}. Finally, a plot of the variation of optimal dimensionless power with the dimensionless Coulomb friction coefficients for a given set of dimensionless viscous friction coefficients is presented in Fig. **4.10**. There is no particular trend observed in the variation of π_1 with π_{14} and π_{15}, but the dimensionless power consumption for a given set of dimensionless tangential and normal Coulomb friction coefficients is in general higher than the dimensionless power consumption for pure viscous friction model i.e. zero Coulomb friction.

Having established the variation of optimal parameters with the Coulomb friction coefficients, experiments are performed on the snake robot to validate these results. However, on the treadmill, the actual friction coefficients C_{t_0}, C_{n_0}, C_t and C_n are constant rather than their dimensionless counterparts. Hence the dimensionless friction coefficients change from one value of omega to another, with the ratios of viscous and Coulomb friction coefficients remaining constant. This is essentially the same problem that was dealt with in Chapter 3 (Tabs. **3.2** - **3.4**) i.e., variation of optimal parameters with the dimensionless friction coefficients while maintaining the friction ratio constant. Table **4.2** represents the variation of optimal parameters with dimensionless friction coefficients. It can however be seen that the optimal parameters α_{opt} and β_{opt} do not

vary much with dimensionless friction coefficients for a given set of friction ratios. This further corroborates the results established in chapter 3.

Tests are performed on the treadmill to validate the frequency-velocity relationship at the optimal parameter settings. The optimal parameters of Tab. **4.2** are used to operate the snake at different frequencies and the velocity of forward locomotion is measured and tabulated along with the corresponding velocity predicted by the analytical model and is presented in Tab. **4.3**. A plot of the analytical and experimental velocities predicted is shown in Fig. **4.11** along with the corresponding curve fits. The experimental velocity measured seems to match closely with the analytical predictions. The slight variations in the values predicted by the experiment can be attributed to the difficulty in predicting the friction characteristics of the snake in the normal direction. Normal friction characteristics are relatively more sensitive to minor variations in the angle λ, while the tangential friction characteristics are independent and these differences get amplified at higher frequencies.

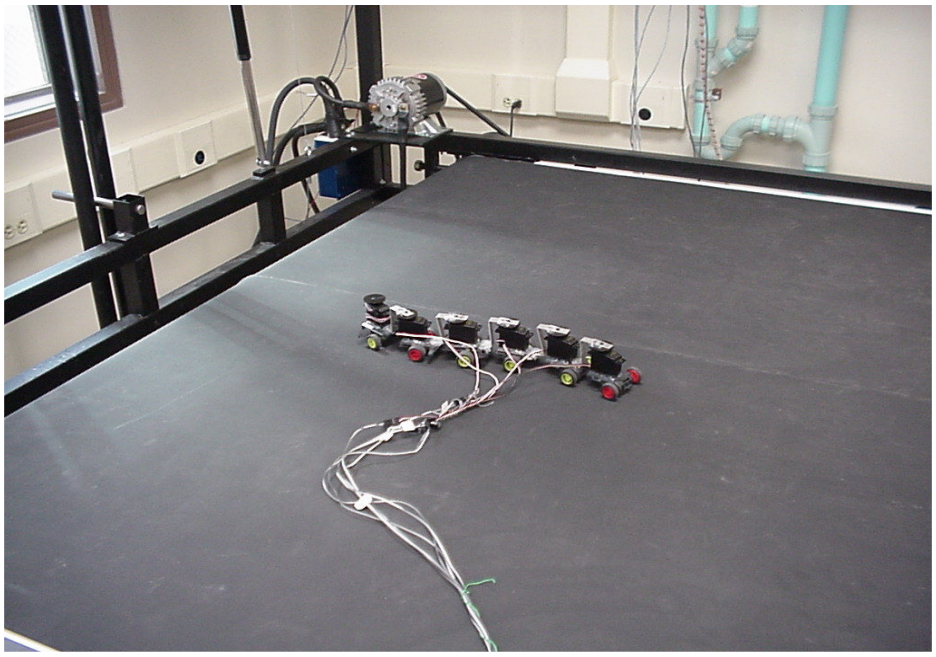

Figure **4.1**: Six-link robotic snake on treadmill

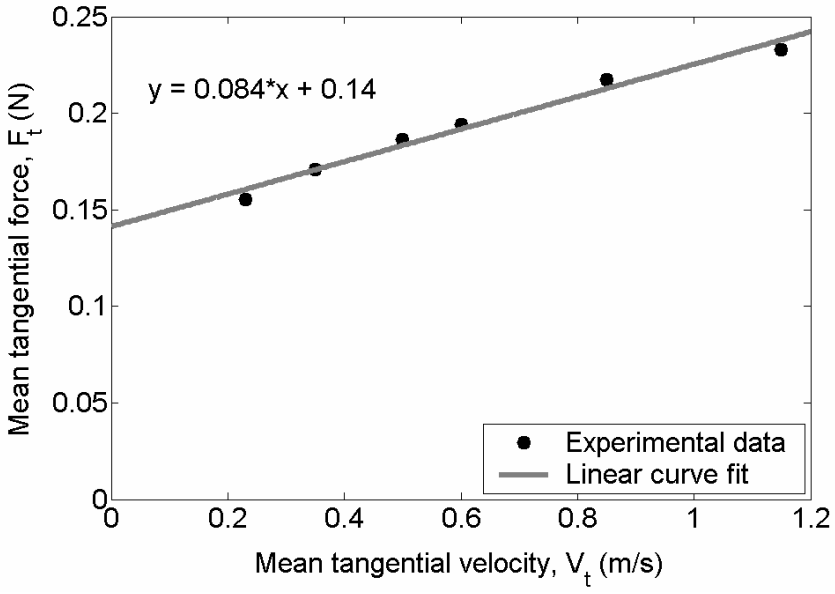

Figure **4.2**: Plot of mean tangential (or longitudinal) force, F_t versus mean tangential (or forward) velocity V_t to determine the tangential friction coefficient, C_t

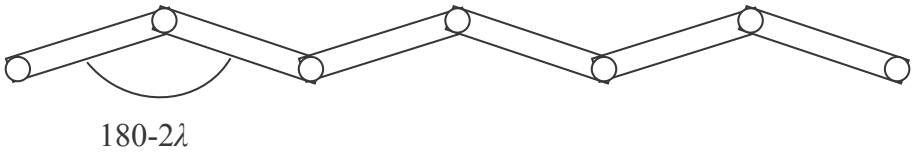

Figure **4.3**: Orientation of the links to determine the normal friction characteristics

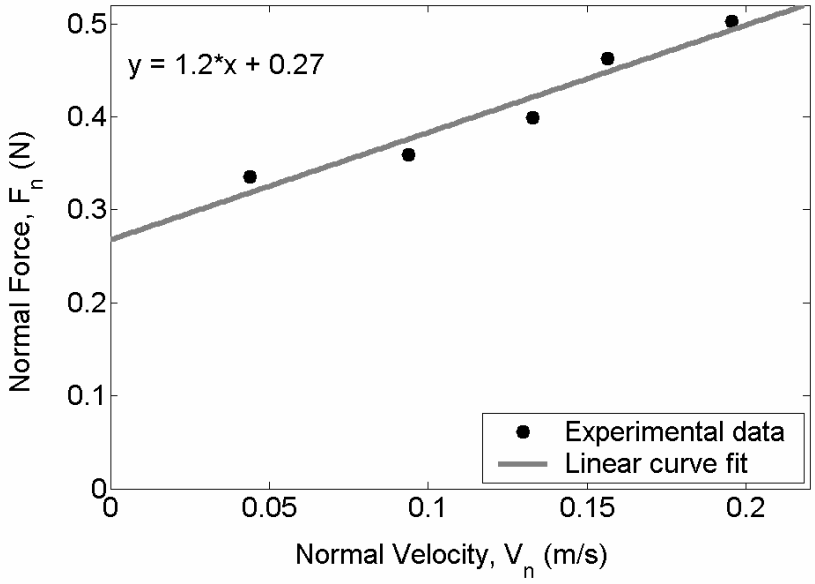

Figure **4.4**: Plot of the mean normal (or transverse) force, F_n versus the mean normal (or transverse) velocity V_n to determine the normal friction coefficient, C_n

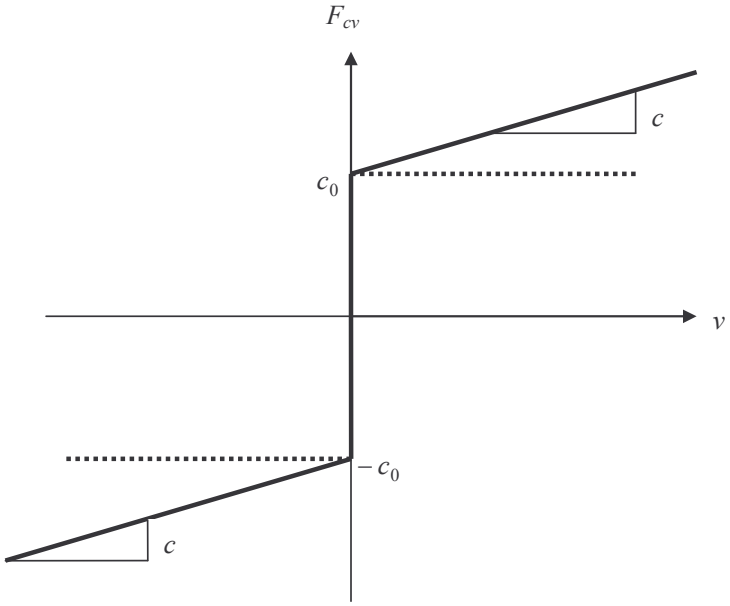

Figure **4.5**:Coulomb plus viscous friction model

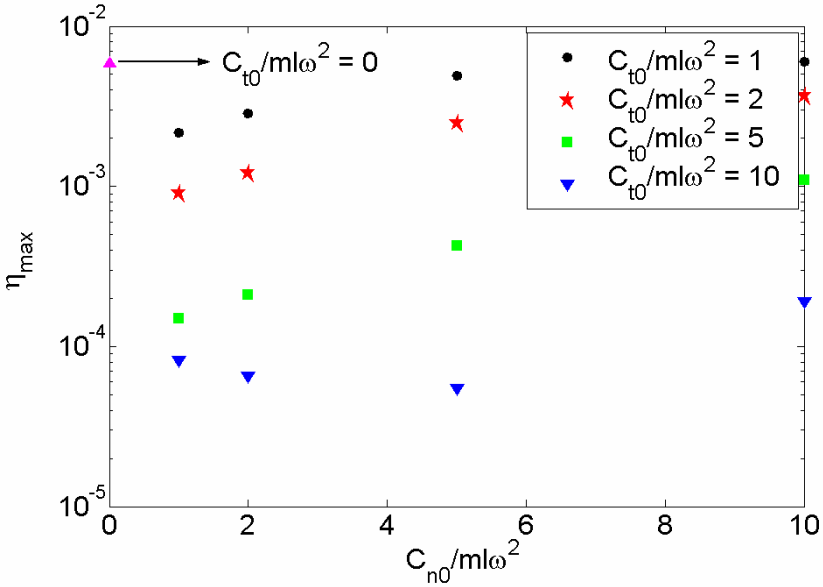

Figure **4.6**: Plot of the variation of η_{max} with dimensionless Coulomb friction coefficients π_{14} and π_{15} while maintaining π_5 and π_6 constant at 1 and 10 respectively

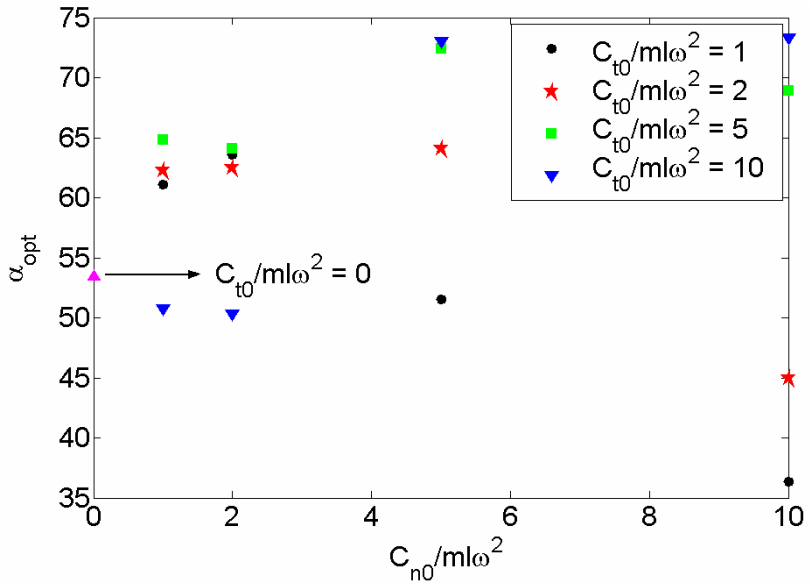

Figure **4.7**: Plot of the variation of α_{opt} with dimensionless Coulomb friction coefficients π_{14} and π_{15} while maintaining π_5 and π_6 constant at 1 and 10 respectively

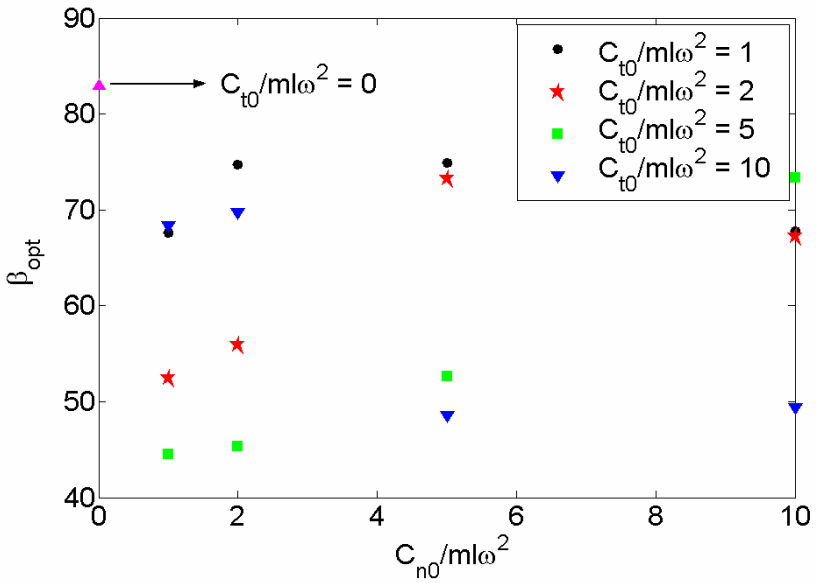

Figure **4.8**: Plot of the variation of β_{opt} with dimensionless Coulomb friction coefficients π_{14} and π_{15} while maintaining π_5 and π_6 constant at 1 and 10 respectively

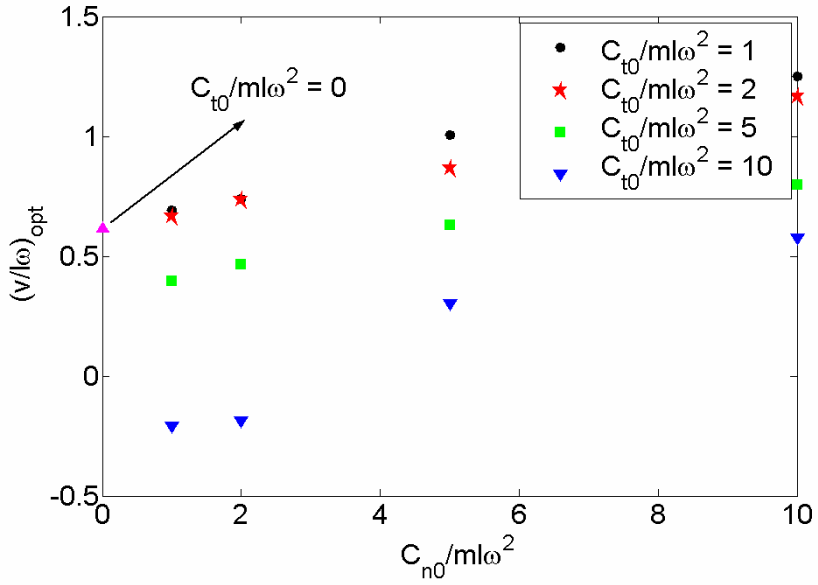

Figure **4.9**: Plot of the variation of optimal dimensionless velocity (π_2) with π_{14} and π_{15} while maintaining π_5 and π_6 constant at 1 and 10 respectively

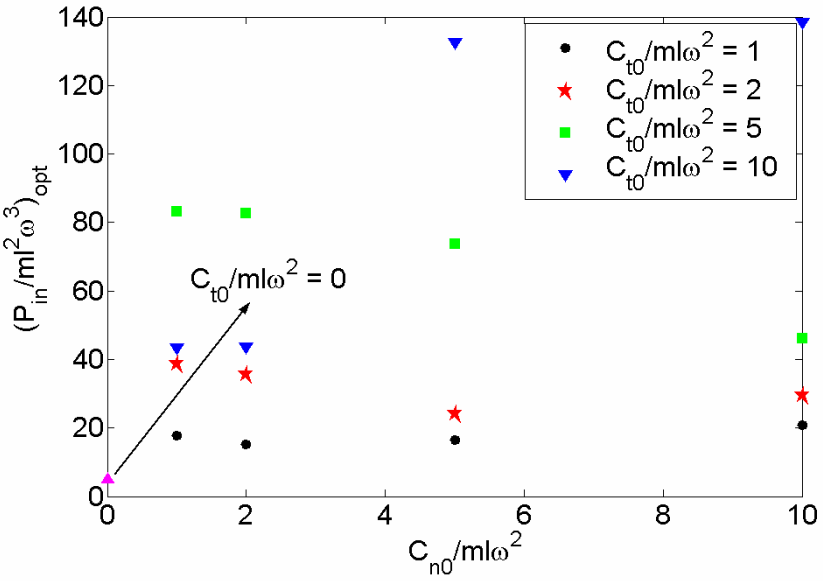

Figure **4.10**: Plot of the variation of optimal dimensionless power (π_1) with π_{14} and π_{15} while maintaining π_5 and π_6 constant at 1 and 10 respectively

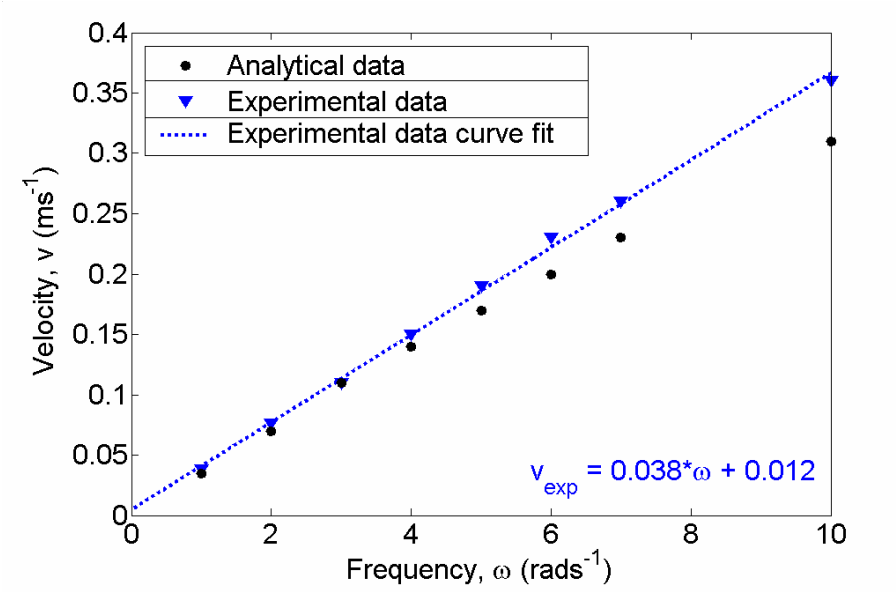

Figure **4.11**: Plot of the variation of analytical and experimental velocity as a function of ω at the optimal parameter setting corresponding to experimental friction model

Table **4.1**: Variation of the optimal parameters with dimensionless Coulomb friction coefficients, π_{14} and π_{15} while maintaining the dimensionless viscous friction coefficients π_5 and π_6 constant at 1 and 10 respectively

π_{14}	π_{15}	α_{opt} (deg)	β_{opt} (deg)	$\eta_{\max}$	$\pi_2 = \frac{v}{l\omega}$	$\pi_1 = \frac{P_{in}}{ml^2\omega^3}$
0	0	53.462	82.968	$5.871*10^{-3}$	0.613	5.098
1	1	61.090	67.5576	$2.166*10^{-3}$	0.693	17.660
	2	63.552	74.7369	$2.871*10^{-3}$	0.738	15.089
	5	51.564	74.8673	$4.886*10^{-3}$	1.005	16.471
	10	36.370	67.8002	$5.987*10^{-3}$	1.251	20.806
2	1	62.255	52.453	$9.115*10^{-4}$	0.665	38.649
	2	62.490	55.9522	$1.204*10^{-3}$	0.734	35.616
	5	64.060	73.2438	$2.482*10^{-3}$	0.867	24.093
	10	44.982	67.2627	$3.679*10^{-3}$	1.167	29.470
5	1	64.784	44.5561	$1.495*10^{-4}$	0.395	83.169
	2	64.102	45.3546	$2.088*10^{-4}$	0.465	82.539
	5	72.388	52.6545	$4.270*10^{-4}$	0.629	73.671
	10	68.905	73.3142	$1.101*10^{-3}$	0.799	46.168
10	1	50.741	68.3025	$8.145*10^{-5}$	-0.210	43.190
	2	50.285	69.737	$6.490*10^{-5}$	-0.188	43.451
	5	72.972	48.4928	$5.422*10^{-5}$	0.300	132.506
	10	73.288	49.3475	$1.896*10^{-4}$	0.574	138.426

Table **4.2**: Variation of the optimal gait parameters with frequency maintaining the friction coefficients constant at the experimentally determined values: $C_t = 0.084$, $C_n = 1.20$, $C_{t_0} = 0.14$ and $C_{n_0} = 0.27$

ω (rad/s)	α_{opt} (deg)	β_{opt} (deg)	$\pi_2 = \frac{v}{l\omega}$	v	π_5 $(\pi_6 = 15 \cdot \pi_5)$	π_{14} $(\pi_{15} = 2 \cdot \pi_{14})$
3.16	69	73	0.92	0.11	0.35	5.0
5	66	73	0.88	0.17	0.22	2.0
7.07	66	72	0.86	0.23	0.16	1.0
10	68	75	0.80	0.31	0.11	0.5
15.81	62	74	0.72	0.43	0.07	0.2

Table **4.3**: Experimental determination of the variation of velocity with frequency on the treadmill at the optimal values predicted by the analytical model

ω (rad/s)	α_{opt} (deg)	β_{opt} (deg)	Analytical velocity (v_{ana})	Experimental velocity ($v_{\exp}$)
1	69	73	0.035	0.042
2	66	73	0.070	0.083
3	66	75	0.11	0.13
4	68	75	0.14	0.17
5	66	73	0.17	0.21
6	68	75	0.20	0.25
7	68	72	0.23	0.28
10	68	75	0.31	0.38

Chapter 5

CONTINUUM SNAKE ROBOT MODEL

5.1 Finite element formulation of the governing dynamics

A mathematical model for continuum snake robot is based on utilizing the beam bending theory to emulate serpentine locomotion. An elementary beam model consists of two degrees of freedom at each node, the transverse displacement and rotation. In addition, an axial degree of freedom at each node should be considered to account for forward motion. Similar to the applied joint torques in an articulated model considered in Chapter 2, the continuum model has bending moments applied to each beam element. Fig. **5.1** shows a five-element (or an 18-degrees of freedom) finite element model used in the design of a continuous snake and Fig. **5.2** describes the nodal parameters of a generic link. The gait of continuum model is first studied in the absence of friction by comparing it to that of a rigid-link model established in Chapter 2. This is achieved by ignoring friction while formulating the governing equations of motion of the flexible snake robot. A viscous friction model is then incorporated into the governing equations to explore locomotion patterns. A five element flexible beam model is assumed to be equivalent to a six-link articulated model based on the fact that each beam element is an actuator in itself.

From the elementary finite element beam theory [**27**], beam element mass and stiffness matrices and force and displacement vectors can be written as follows:

The element mass matrix, $[m]$ is defined as:

$$[m]=\frac{\rho Al}{420}\begin{bmatrix} 140 & 0 & 0 & 70 & 0 & 0 \\ 0 & 156 & 22l & 0 & 54 & -13l \\ 0 & 22l & 4l^2 & 0 & 13l & -3l^2 \\ 70 & 0 & 0 & 140 & 0 & 0 \\ 0 & 54 & 13l & 0 & 156 & -22l \\ 0 & -13l & -3l^2 & 0 & -22l & 4l^2 \end{bmatrix} \tag{5.1}$$

The element stiffness matrix, $[k]$ is given by:

$$[k]=\begin{bmatrix} C_1 & 0 & 0 & -C_1 & 0 & 0 \\ 0 & 12C_2 & 6C_2l & 0 & -12C_2l & 6C_2l \\ 0 & 6C_2l & 4C_2l^2 & 0 & -6C_2l & 2C_2l^2 \\ -C_1 & 0 & 0 & C_1 & 0 & 0 \\ 0 & -12C_2 & -6C_2l & 0 & 12C_2 & -6C_2l \\ 0 & 6C_2l & 2C_2l^2 & 0 & -6C_2l & 4C_2l^2 \end{bmatrix} \tag{5.2}$$

where C_1 and C_2 are defined as follows:

$$C_1=\frac{EA}{l}$$
$$C_2=\frac{EI}{l^3} \tag{5.3}$$

The element force vector, f_e comprises of the externally applied forces and moments to the beam element. Since there are no external forces applied to the beam element and only bending moments are applied to the beam element as shown in Fig. **5.2**. The external force vector for i^{th} beam element is given by:

$$\{f_e\} = \begin{Bmatrix} 0 \\ 0 \\ M_i \\ 0 \\ 0 \\ -M_i \end{Bmatrix} \tag{5.4}$$

with applied bending moment assumed to be of the form:

$$M_i = M_0 \sin(\omega t + \beta_i) \tag{5.5}$$

where, $\beta_i = (i-1)\beta$ and $i = 1, 2, \ldots n$

The element friction vector, f_{fric}, is derived from the non-conservative work done in overcoming friction. Based on the viscous friction model developed in Chapter 2, i.e. Eqs. (**2.28** - **2.33**), the frictional losses can be derived. The friction forces at any given point on a beam element are depicted in the local (t - n) and global (x - y) frames of reference in Fig. **5.3**. The work expended (per unit length) in overcoming the contact forces between the ground and an infinitesimal element length can be expressed in the global coordinate system as follows:

$$\delta\overline{W}_f = \delta u \cdot \overline{F}_x + \delta w \cdot \overline{F}_y \tag{5.6}$$

where, $\overline{W}_f$ is the work done per unit length; $\overline{F}_x$ and $\overline{F}_y$ are frictional forces per unit element length and δu and δw are the infinitesimal displacements in x and y directions respectively.

Equation (**5.6**) can be rewritten in matrix form as:

$$\delta\overline{W}_f = \begin{bmatrix} \delta u & \delta w \end{bmatrix} \cdot \begin{Bmatrix} \overline{F}_x \\ \overline{F}_y \end{Bmatrix} \tag{5.7}$$

Using a similar form of Eq. (**2.33**) in Eq. (**5.7**) results in:

$$\delta \overline{W}_f = -\begin{bmatrix}\delta u & \delta w\end{bmatrix} \cdot \begin{bmatrix}\cos\theta & -\sin\theta \\ \sin\theta & \cos\theta\end{bmatrix} \cdot \begin{bmatrix}\overline{C}_t & 0 \\ 0 & \overline{C}_n\end{bmatrix} \cdot \begin{bmatrix}\cos\theta & \sin\theta \\ -\sin\theta & \cos\theta\end{bmatrix} \cdot \begin{Bmatrix}\dot{u} \\ \dot{w}\end{Bmatrix} \tag{5.8}$$

where $\overline{C}_t$ and $\overline{C}_n$ are the tangential and normal friction coefficients per unit length.

The total energy lost in overcoming friction and hence the element friction matrix is obtained by integrating Eq. (**5.8**) over the element length. This procedure is detailed in Section **5.3** where locomotion of a continuous snake is analyzed.

The element displacement vector consists of nodal translational and rotational displacements and is given as:

$$\{x\} = \begin{Bmatrix} u_1 \\ w_1 \\ \theta_1 \\ u_2 \\ w_2 \\ \theta_2 \end{Bmatrix} \tag{5.9}$$

where the various parameters used in Eqs. (**5.1** - **5.9**) are defined as follows:

n	Total number of beam elements
ρ	Mass density of each beam element
A	Cross-sectional area of the beam
l	Length of the beam element
E	Modulus of elasticity
I	Area moment of inertia of the beam cross section
M_i	Moment applied to the i^{th} beam element

u_i, w_i, θ_i Linear and angular displacements of the i^{th} node

M_0 Magnitude of the applied bending moment to the i^{th} element

ω Frequency of sine-wave input

β Relative phase lag between the sinusoidal inputs of the adjacent beam elements

The element matrices are assembled, assuming identical properties for all the elements, to arrive at the global matrices and hence the global equations of motion. These global equations of motion can be expressed as follows:

$$[M]\{\ddot{X}\} + [K]\{X\} = \{F_e\} + \{F_{fric}\} \quad (5.10)$$

where

M Global mass matrix

K Global stiffness matrix

F_e Global load vector

F_{fric} Global friction vector

X Global displacement vector

The MATLAB Simulink software is used to numerically integrate Eq. (5.10) to obtain a solution $X(t)$. Fig. 5.4 represents the implementation of the dynamics of a continuum model in MATLAB Simulink software. After obtaining the nodal displacement vector, $X(t)$, the variation of translational and rotational displacements between any two adjacent nodes is determined by using the appropriate shape functions. The variation of the longitudinal displacement, $u(\xi, t)$ over the element length and as a function of time is given as:

$$u(\xi,t)=\begin{bmatrix}N_{u1}(\xi) & N_{u2}(\xi)\end{bmatrix}\cdot\begin{Bmatrix}u_1(t)\\ u_2(t)\end{Bmatrix} \tag{5.11}$$

where the linear shape functions $N_{u1}(\xi)$, $N_{u2}(\xi)$ utilized above are described as follows:

$$\begin{aligned}N_{u1}&=\frac{1}{2}(1-\xi)\\ N_{u2}&=\frac{1}{2}(1+\xi)\end{aligned} \tag{5.12}$$

with

$$\xi=\frac{2x}{l}-1 \tag{5.13}$$

being the dimensionless coordinate along the length of a beam element. The coordinate ξ as seen in Fig. **5.2** varies from ξ = -1 at node 1 (x = 0) to ξ = +1 at node 2 (x = l).

Similarly, the variation of transverse displacement between two adjacent nodes of an element is given by:

$$w(\xi,t)=\begin{bmatrix}N_{w1}(\xi) & N_{\theta1}(\xi) & N_{w2}(\xi) & N_{\theta2}(\xi)\end{bmatrix}\cdot\begin{Bmatrix}w_1(t)\\ \theta_1(t)\\ w_2(t)\\ \theta_2(t)\end{Bmatrix} \tag{5.14}$$

where the cubic shape functions of a plane beam element used to interpolate between any two adjacent nodes of an element are given by:

$$\begin{aligned}N_{w1}&=\frac{1}{4}(1-\xi)^2(2+\xi)\\ N_{\theta1}&=\frac{1}{8}l(1-\xi)^2(1+\xi)\\ N_{w2}&=\frac{1}{4}(1+\xi)^2(2-\xi)\\ N_{\theta2}&=-\frac{1}{8}l(1+\xi)^2(1-\xi)\end{aligned} \tag{5.15}$$

Finally, the rotation between two adjacent nodes is governed by:

$$\theta(\xi,t)=\frac{d}{dx}w(\xi,t) \tag{5.16}$$

which can be rewritten as:

$$\theta(\xi,t)=\frac{d}{d\xi}w(\xi,t)\cdot\frac{d\xi}{dx} \tag{5.17}$$

Further, differentiating Eq. (**5.13**) with respect to *x* yields:

$$\frac{d\xi}{dx}=\frac{2}{l} \tag{5.18}$$

Substituting Eqs. (**5.14**, **5.15** and **5.18**) in Eq. (**5.17**) results in:

$$\theta(\xi,t)=\frac{2}{l}\cdot\left[\frac{d}{d\xi}\{N_{w1}(\xi)\}\quad\frac{d}{d\xi}\{N_{\theta1}(\xi)\}\quad\frac{d}{d\xi}\{N_{w2}(\xi)\}\quad\frac{d}{d\xi}\{N_{\theta2}(\xi)\}\right]\cdot\begin{Bmatrix}w_1(t)\\ \theta_1(t)\\ w_2(t)\\ \theta_2(t)\end{Bmatrix} \tag{5.19}$$

Upon simplification, this results in:

$$\theta(\xi,t)=\frac{2}{l}\left[B_{w1}(\xi)\quad B_{\theta1}(\xi)\quad B_{w2}(\xi)\quad B_{\theta2}(\xi)\right]\cdot\begin{Bmatrix}w_1(t)\\ \theta_1(t)\\ w_2(t)\\ \theta_2(t)\end{Bmatrix} \tag{5.20}$$

where the quadratic interpolation functions are given as:

$$\begin{aligned}B_{w1}&=\frac{3}{2l}(\xi-1)(\xi+1)\\ B_{\theta1}&=\frac{1}{4}(3\xi+1)(\xi-1)\\ B_{w2}&=-\frac{3}{2l}(\xi-1)(\xi+1)\\ B_{\theta2}&=\frac{1}{4}(3\xi+1)(\xi-1)\end{aligned} \tag{5.21}$$

Equations (**5.11**, **5.14** and **5.20**) can be assembled together into one single equation that describes the variations of displacements and rotations as a function of time and element length as follows:

$$\begin{Bmatrix} u(\xi,t) \\ w(\xi,t) \\ \theta(\xi,t) \end{Bmatrix} = \begin{bmatrix} N_{u1}(\xi) & 0 & 0 & N_{u2}(\xi) & 0 & 0 \\ 0 & N_{w1}(\xi) & N_{\theta 1}(\xi) & 0 & N_{w2}(\xi) & N_{\theta 2}(\xi) \\ 0 & B_{w1}(\xi) & B_{\theta 1}(\xi) & 0 & B_{w2}(\xi) & B_{\theta 2}(\xi) \end{bmatrix} \cdot \begin{Bmatrix} u_1(t) \\ w_1(t) \\ \theta_1(t) \\ u_2(t) \\ w_2(t) \\ \theta_2(t) \end{Bmatrix} \qquad (5.22)$$

Thus, using the Global displacement vector, $X(t)$ obtained from Simulink and the shape functions described by Eq. (**5.22**), the beam's displacement and rotation at any time instant can be determined.

5.2 Gait comparison to a discrete snake model

As stated earlier, to compare the gait of a continuum model to that of a rigid link snake robot established in chapter 2, friction is neglected. Thus the governing equations of motion established in Eq. (**5.10**) take the form:

$$[M]\{\ddot{X}\} + [K]\{X\} = \{F\} \qquad (5.23)$$

The dynamics of the above system are simulated using Simulink software and a plot of the snake's gait at six time instances over one time period for phase angle, β = 80 deg, and frequency, ω = 3 rads^{-1}is shown in Fig. **5.5** A similar plot is made for the rigid-link snake robot and is shown in Fig. **5.6**. The total mass and length of the snake are maintained the same between the two models.

Comparing Figs. **5.5** and **5.6**, one can conclude that the gait of the continuum snake matches closely to the rigid-link snake. A six-link articulated model is equivalent to a five-link flexible model as stated earlier. In order to match the transverse displacement of the flexible snake to that of a rigid-link snake, tuning of the beam bending rigidity and (or) the applied bending moment is necessary.

5.3 Introduction to locomotion

The locomotion of a continuum snake robot is analyzed by employing a viscous friction model to describe the element-to-ground interaction as in the case of an articulated model. Eq. (**5.8**) established earlier has to be integrated over the element length to obtain the element friction vector. Using Eqs. (**5.11**) and (**5.14**), $\delta u, \dot{u}, \delta w$ and $\dot{w}$ can be expressed as follows:

$$\delta u = \begin{bmatrix} N_{u1} & N_{u2} \end{bmatrix} \cdot \begin{Bmatrix} \delta u_1 \\ \delta u_2 \end{Bmatrix} \tag{5.24}$$

$$\dot{u} = \begin{bmatrix} N_{u1} & N_{u2} \end{bmatrix} \cdot \begin{Bmatrix} \dot{u}_1 \\ \dot{u}_2 \end{Bmatrix} \tag{5.25}$$

$$\delta w = \begin{bmatrix} N_{w1} & N_{\theta 1} & N_{w2} & N_{\theta 2} \end{bmatrix} \cdot \begin{Bmatrix} \delta w_1 \\ \delta \theta_1 \\ \delta w_2 \\ \delta \theta_2 \end{Bmatrix} \tag{5.26}$$

and

$$\dot{w} = \begin{bmatrix} N_{w1} & N_{\theta 1} & N_{w2} & N_{\theta 2} \end{bmatrix} \cdot \begin{Bmatrix} \dot{w}_1 \\ \dot{\theta}_1 \\ \dot{w}_2 \\ \dot{\theta}_2 \end{Bmatrix} \tag{5.27}$$

Combining Eqs. (5.24) and (5.26) into a single equation results in:

$$\begin{bmatrix} \delta u & \delta w \end{bmatrix} = \begin{bmatrix} \delta u_1 & \delta w_1 & \delta \theta_1 & \delta u_2 & \delta w_2 & \delta \theta_2 \end{bmatrix} \cdot \begin{bmatrix} N_{u1} & 0 \\ 0 & N_{w1} \\ 0 & N_{\theta 1} \\ N_{u2} & 0 \\ 0 & N_{w2} \\ 0 & N_{\theta 2} \end{bmatrix} \tag{5.28}$$

Similarly, combining Eqs. (5.25) and (5.27) yields:

$$\begin{Bmatrix} \dot{u} \\ \dot{w} \end{Bmatrix} = \begin{bmatrix} N_{u1} & 0 & 0 & N_{u2} & 0 & 0 \\ 0 & N_{w1} & N_{\theta 1} & 0 & N_{w2} & N_{\theta 2} \end{bmatrix} \cdot \begin{Bmatrix} \dot{u}_1 \\ \dot{w}_1 \\ \dot{\theta}_1 \\ \dot{u}_2 \\ \dot{w}_2 \\ \dot{\theta}_2 \end{Bmatrix} \tag{5.29}$$

Substituting Eqs. (5.28) and (5.29) into Eq. (5.8) yields:

$$\delta\overline{W}_f = -\begin{bmatrix}\delta u_1 & \delta w_1 & \delta\theta_1 & \delta u_2 & \delta w_2 & \delta\theta_2\end{bmatrix}\cdot\begin{bmatrix}N_{u1} & 0\\ 0 & N_{w1}\\ 0 & N_{\theta1}\\ N_{u2} & 0\\ 0 & N_{w2}\\ 0 & N_{\theta2}\end{bmatrix}\cdot\begin{bmatrix}\cos\theta & -\sin\theta\\ \sin\theta & \cos\theta\end{bmatrix}\cdot$$

$$\begin{bmatrix}\overline{C}_t & 0\\ 0 & \overline{C}_n\end{bmatrix}\cdot\begin{bmatrix}\cos\theta & \sin\theta\\ -\sin\theta & \cos\theta\end{bmatrix}\cdot\begin{bmatrix}N_{u1} & 0 & 0 & N_{u2} & 0 & 0\\ 0 & N_{w1} & N_{\theta1} & 0 & N_{w2} & N_{\theta2}\end{bmatrix}\cdot\begin{Bmatrix}\dot{u}_1\\ \dot{w}_1\\ \dot{\theta}_1\\ \dot{u}_2\\ \dot{w}_2\\ \dot{\theta}_2\end{Bmatrix} \tag{5.30}$$

Integrating Eq. (5.30) over element length yields:

$$\int_0^L\left(\delta\overline{W}_f\right)dx = -\int_0^L\left(\begin{bmatrix}\delta u_1 & \delta w_1 & \delta\theta_1 & \delta u_2 & \delta w_2 & \delta\theta_2\end{bmatrix}\cdot\begin{bmatrix}N_{u1} & 0\\ 0 & N_{w1}\\ 0 & N_{\theta1}\\ N_{u2} & 0\\ 0 & N_{w2}\\ 0 & N_{\theta2}\end{bmatrix}\cdot\right.$$

$$\begin{bmatrix}\cos\theta & -\sin\theta\\ \sin\theta & \cos\theta\end{bmatrix}\cdot\begin{bmatrix}\overline{C}_t & 0\\ 0 & \overline{C}_n\end{bmatrix}\cdot\begin{bmatrix}\cos\theta & \sin\theta\\ -\sin\theta & \cos\theta\end{bmatrix}\cdot \tag{5.31}$$

$$\left.\begin{bmatrix}N_{u1} & 0 & 0 & N_{u2} & 0 & 0\\ 0 & N_{w1} & N_{\theta1} & 0 & N_{w2} & N_{\theta2}\end{bmatrix}\cdot\begin{Bmatrix}\dot{u}_1\\ \dot{w}_1\\ \dot{\theta}_1\\ \dot{u}_2\\ \dot{w}_2\\ \dot{\theta}_2\end{Bmatrix}\right)dx$$

Simplifying Eq. (5.31) using Eq. (5.18) results in:

$$\delta W_f = -\frac{l}{2}\cdot\begin{bmatrix}\delta u_1 & \delta w_1 & \delta\theta_1 & \delta u_2 & \delta w_2 & \delta\theta_2\end{bmatrix}\cdot\left\{\int_{-1}^{1}\left(\begin{bmatrix}N_{u1} & 0\\ 0 & N_{w1}\\ 0 & N_{\theta1}\\ N_{u2} & 0\\ 0 & N_{w2}\\ 0 & N_{\theta2}\end{bmatrix}\cdot\begin{bmatrix}\cos\theta & -\sin\theta\\ \sin\theta & \cos\theta\end{bmatrix}\cdot\begin{bmatrix}\overline{C}_t & 0\\ 0 & \overline{C}_n\end{bmatrix}\cdot\begin{bmatrix}\cos\theta & \sin\theta\\ -\sin\theta & \cos\theta\end{bmatrix}\cdot\begin{bmatrix}N_{u1} & 0 & 0 & N_{u2} & 0 & 0\\ 0 & N_{w1} & N_{\theta1} & 0 & N_{w2} & N_{\theta2}\end{bmatrix}\right)d\xi\right\}\cdot\begin{Bmatrix}\dot{u}_1\\ \dot{w}_1\\ \dot{\theta}_1\\ \dot{u}_2\\ \dot{w}_2\\ \dot{\theta}_2\end{Bmatrix} \tag{5.32}$$

where W_f is the total energy expended in overcoming the contact forces between the ground and beam element. Eq. (**5.32**) can be rewritten utilizing Eq. (**5.9**) as follows:

$$\delta W_f = \delta\{x\}\cdot\left(-\frac{l}{2}\int_{-1}^{1}[D]'\cdot[T]'\cdot[G]\cdot[T]\cdot[D]d\xi\right)\cdot\{\dot{x}\} \tag{5.33}$$

where, the shape function matrix, D, the transformation matrix, T, and the friction coefficient matrix, G are defined as:

$$D = \begin{bmatrix}N_{u1} & 0 & 0 & N_{u2} & 0 & 0\\ 0 & N_{w1} & N_{\theta1} & 0 & N_{w2} & N_{\theta2}\end{bmatrix}$$

$$T = \begin{bmatrix}\cos\theta & \sin\theta\\ -\sin\theta & \cos\theta\end{bmatrix} \tag{5.34}$$

$$G = \begin{bmatrix}\overline{C}_t & 0\\ 0 & \overline{C}_n\end{bmatrix}$$

Eq. (**5.33**) is of the form:

$$\delta W_f = \delta\{x\} \cdot f_{fric} \tag{5.35}$$

The element friction matrix, f_{fric}, is given by:

$$f_{fric} = \left(-\frac{l}{2} \int_{-1}^{1} [D]' \cdot [T]' \cdot [G] \cdot [T] \cdot [D] d\xi \right) \cdot \{\dot{x}\} \tag{5.36}$$

which is of the form,

$$f_{fric} = -[c] \cdot \{\dot{x}\} \tag{5.37}$$

where $[c]$ is analogous to element damping matrix and is of the same dimensions (6x6) as the element mass and stiffness matrices and is given by:

$$[c] = \frac{l}{2} \int_{-1}^{1} [D]' \cdot [T]' \cdot [G] \cdot [T] \cdot [D] d\xi \tag{5.38}$$

Due to the non-linear nature of the integrand in Eq. (**5.38**), numerical integration is carried out to determine the $[c]$ matrix. The element damping matrices are then assembled assuming identical properties for all the elements, to arrive at the global damping matrix, $[C]$ Thus, the global equations of motion for a beam element as indicated in Eq. (**5.10**) can be simplified using Eq. (**5.37**) as:

$$[M]\{\ddot{X}\} + [K]\{X\} + [C]\{\dot{X}\} = \{F_e\} \tag{5.39}$$

where $[C]$ is equivalent to global damping matrix.

Eq. (**5.39**) is solved numerically using MATLAB Simulink software to obtain the nodal displacements and rotations of the beam elements as a function of time. A plot of the snake's gait at β = 81 deg and ω = 5 rads^{-1} at five instances over one time period is shown in Fig. **5.7**. A trace of the path followed by the snake robot at β = 81 deg and ω =

5 rads^{-1} is presented in Fig. **5.8**. Similar plots for the rigid-link snake robot are presented in Chapter 2. The total mass and length of the snake as well the overall friction characteristics are maintained the same between the two models.

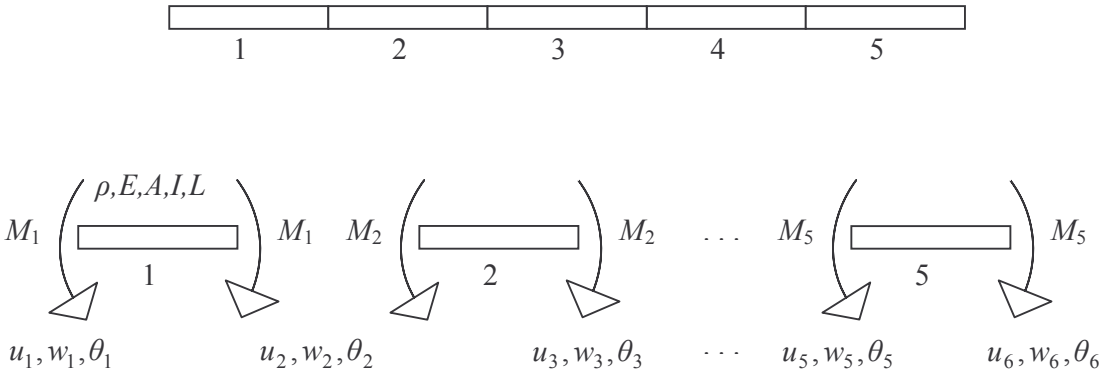

Figure **5.1**: Five-element beam model of continuum snake

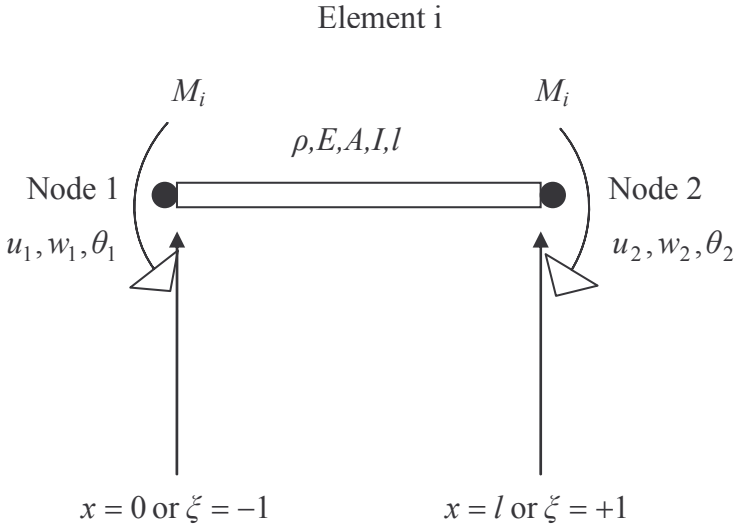

Figure **5.2**: A representation of nodal parameters on the i^{th} element

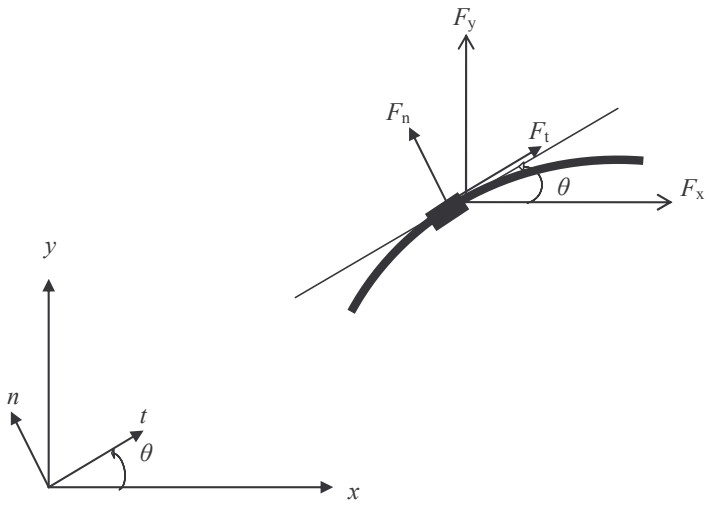

Figure **5.3**: Representation of the friction forces in the local and global coordinates at a given point on a beam element

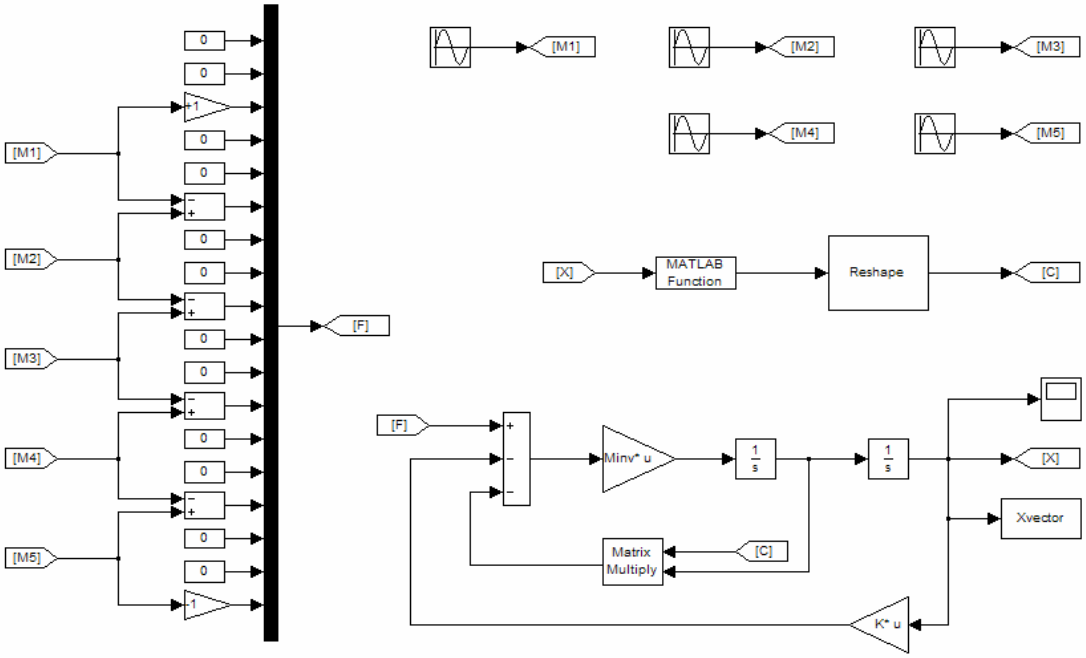

Figure **5.4**: Simulink block diagram implementation of the dynamics of a continuum snake robot model

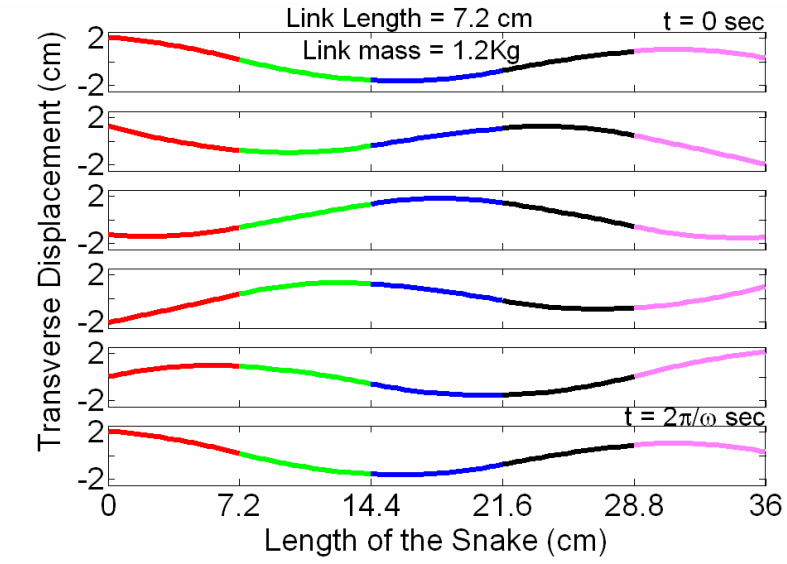

Figure **5.5**: Plot of the gait of continuum model over one time period for β = 80 deg, and ω = 3 rads^{-1} for zero friction case

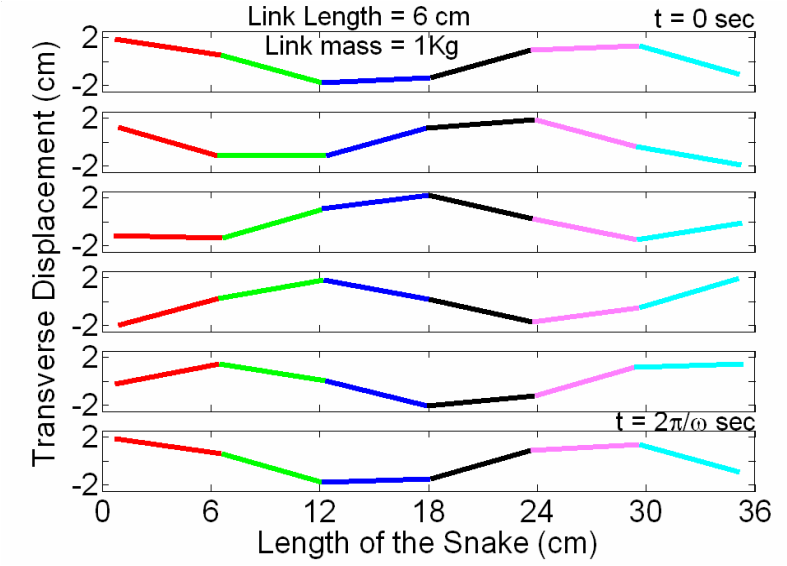

Figure **5.6**: Plot of the gait of discrete model over one time period for β = 80 deg, and ω = 3 rads^{-1} for zero friction case

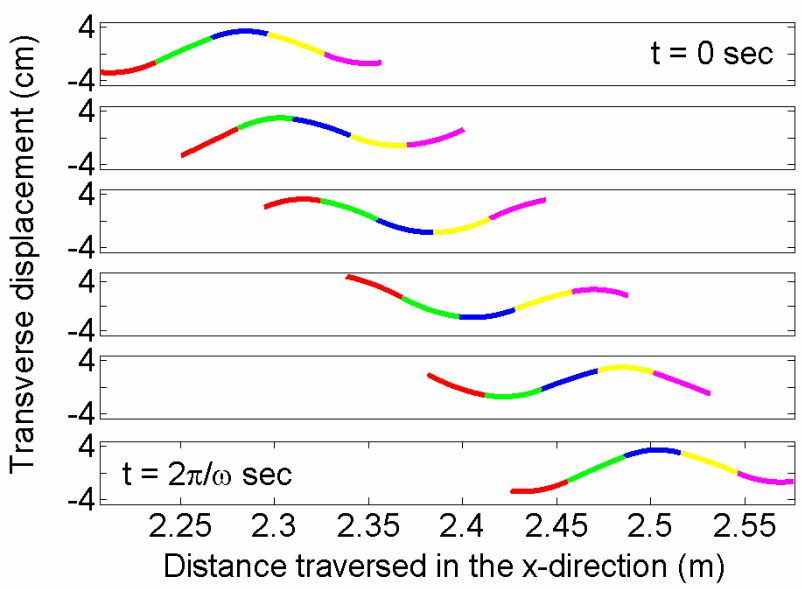

Figure **5.7**: Plot of the continuum snake robot's gait at five instances over one time period at β = 80 deg, and ω = 5 rads^{-1}

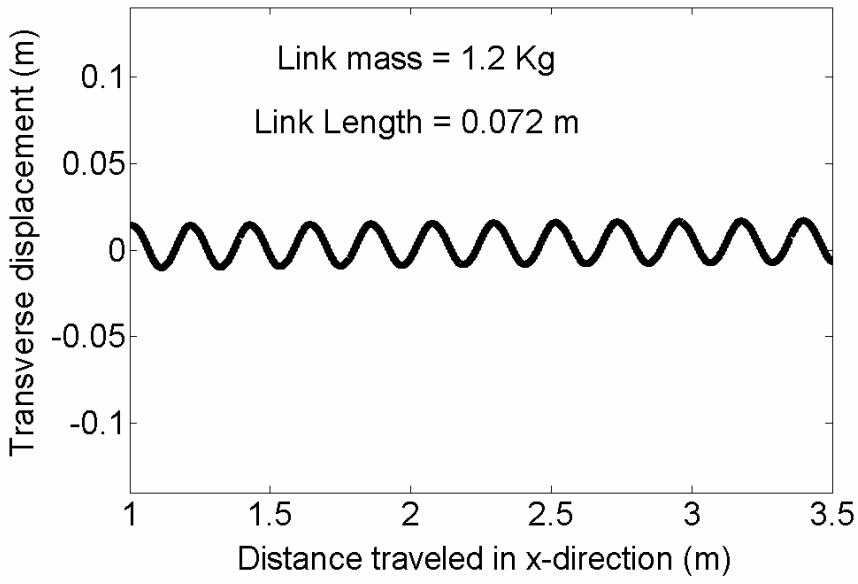

Figure **5.8**: A trace of the path followed by the flexible snake robot at β = 80 deg, and ω = 5 rads^{-1}

Chapter 6

CONCLUSIONS AND FUTURE WORK

6.1 Conclusions

The primary goal of this study has been to develop mathematical models suitable for the analysis, design and control of snake-like locomotors. An implicit method to study the dynamics of serpentine locomotion has been established. Using this implicit model, optimal gait of a six-link snake robot that maximizes the performance index is established for a wide range of friction characteristics. Experimental tests are performed on a six-link robotic snake to validate the optimal gait established via the analytical model. Further, a dynamic model for continuum snake robot is presented with details of the friction modeling and comparisons to rigid-link model.

In Chapter 2, a detailed formulation of the dynamics of a three-link articulated model is presented in two different methods - explicit and implicit. A comparison of the results from the two methods is then presented to confirm that the two methods are equivalent. It is algebraically quite challenging and tedious to solve for the governing equations of motion for higher number of links by the explicit method. The implicit method simplifies the algebraic manipulations considerably by relaxing an algebraic constraint of connection between the joints by modeling them using spring-damper systems. The dynamics of the spring-damper system can be simulated to directly obtain the coupling forces between the joints and hence does not require solving for the joint

forces as in the implicit method. The key advantages of implicit method are that the friction model is not inter-linked with the formulation or derivation of the system dynamics and the ability to extend the theory to higher number of links. This is quite unlike the explicit model where the governing differential equations have to be re-derived to account for the changes in friction characteristics and extending the explicit model to higher number of links is very challenging.

Having established that the implicit model predicts locomotion behavior equally as well as an explicit model for a three-link snake robot, the implicit model is then used in Chapter 3 to establish the optimal gait of a six-link snake robot. Dimensional analysis and Buckingham's pi theorem are used to effectively analyze the optimally efficient locomotion by combining the various parameters influencing the snake's locomotion into a group of dimensionless parameters. In order to determine the optimally efficient gait, two solution methods are considered: 1) an iterative search through a range of parameters α and β and 2) a non-linear multi-variable optimization technique. Although an iterative search method helps in establishing the presence of a unique optimal operating point, it is however numerically quite challenging to determine the optimal parameters using this method. A non-linear multi-variable optimization routine is instead used to predict the optimal gait parameters for varying tangential and normal viscous friction characteristics. The following are some of the important conclusions drawn from the study:

- For maximum performance index, one has to operate at low values of tangential friction coefficient (π_5 between 0.01 and 0.1) and high values of friction ratio ($\frac{\pi_6}{\pi_5}$ between 100 and 1000). The same holds true even for maximum velocity.

- $\eta_{\max}$ in general does not vary as much with the friction ratio as compared to the actual dimensionless value of tangential friction. This is quite unlike the variation in the optimal gait parameter α_{opt}, which is greatly influenced by the friction ratio rather than the magnitude of friction coefficient.
- At lower values of tangential friction, ($\pi_5 < 0.1$) optimal velocity increases with the friction ratio, but at values of $\pi_5 > 0.1$, optimal velocity decreases for higher values of friction ratio ($\frac{\pi_6}{\pi_5} > 100$). This drop in velocity increases for higher values of friction ratio. Furthermore, for a given friction ratio, there is a limit on π_5, and for a given π_5, there is limit on friction ratio, upto which the velocity increases and beyond which it starts decreasing.

Results from the experimental tests performed on a six-link snake robot are presented in Chapter 4. Specifically, friction characteristics of the treadmill are measured and found to resemble that of a Coulomb plus viscous friction model. The variation of the optimal gait parameters with the tangential and normal Coulomb friction coefficients is established maintaining the viscous friction coefficients constant. The maximum performance index in general increases with increasing dimensionless normal Coulomb friction coefficient and decreases with increase in dimensionless tangential friction coefficient. The same trend is also observed in the variation of optimal velocity. β_{opt} for a given set of dimensionless Coulomb friction coefficients is in general less than the value at zero Coulomb friction. This means the optimal motion consists of lesser number of sine waves in the presence of Coulomb friction. Finally, experiments are performed on

the snake robot at the optimal parameters obtained by the analysis and the variation of optimal velocity with frequency is studied. The experimental predictions indicated close agreement with the analytical results.

6.2 Recommendations for Future Work

In the present study a comprehensive theory has been presented that can be used as a foundation for further study of serpentine locomotion. This thesis has however opened up as many questions for future research as it has answered regarding the basic understanding of snake-like locomotion. This section summarizes the areas of possible future research.

1. The variation of optimal parameters with number of links. Specifically how the velocity, power consumption and performance index vary with the number of links; and what would an optimal number of links be to operate on a surface with a given set of friction characteristics to achieve maximum performance index. Does an optimal value for number of links exist? What should be the number of links for end-effects to not have an influence on the joint forces of intermediate links?
2. Robustness of the maximum performance index predicted with uncertainty in system parameters i.e. how would the performance index be affected if the friction characteristics are uncertain or if the power input is limited and how would the optimal gait parameters change.

3. Experimental validation of the power consumption and optimal gait parameters. Although the variation of experimentally measured power consumption matches qualitatively with the analytical results, the exact values could not be matched because of the high standby current consumption of the servo actuators. Other methods to measure the power consumption such that this offset is accounted or eliminated have to be considered.
4. Variation of the optimal gait parameters and the corresponding maximum performance index for a continuum snake robot. It has been observed that even assuming discrete points of contacts with the ground at the nodes, the distance traveled by the snake seemed to be comparable to that of a snake with continuous friction contact with the surface. This issue needs to be further analyzed with regards to performance index to determine whether a discrete friction model would still be enough even for a continuum snake robot.

In addition to the above possible areas of future work based on the currently established models, new mathematical models can be developed to explore the following areas:

5. The present study deals only with the analysis of planar serpentine locomotion. There are however other gaits e.g. sidewinding, concertina and rectilinear that needs to be explored along with three-dimensional motion. The variation of performance index with different gaits; and given a set of friction characteristics, what would be an appropriate gait to operate in to achieve maximum performance index?

6. Effect of other friction models i.e. fluid drag model, Coulomb friction approximation, biviscous friction model etc. on the maximum performance index and other optimal parameters. Additionally, methods to measure or estimate the robot/ground interaction to further improve adaptability to the environment and minimize the power consumption or equivalently maximize the performance index can also be studied. Serpentine locomotion on surfaces with uniform friction characteristics reminiscent of [**17**] is also open to investigation.
7. On the experimental front, friction characteristics can be determined for various other surfaces and the optimal gait parameters established via the analytical model can be validated with the experimental results.
8. Although, a mathematical framework has been established for the analysis of dynamics of a continuum snake robot explicitly, other methods of investigating the flexible robot locomotion is still open to exploration. For instance, is there an implicit method of analyzing the dynamics of a continuum snake similar to the articulated model remains to be answered? This might be of interest in the optimal gait analysis where an implicit method, if existed, may take lesser simulation time than the explicit method.
9. The continuum snake robot analysis can further be extended to adapt to various friction environments and a continuum snake can be built to validate the analytical results.
10. Applications related to grasping, path planning, motion control, obstacle avoidance, etc. can be studied to make the snake robot adapt to environment and perform various tasks.

Bibliography

1 Umetani, Y., and Hirose, S., 1974, "Biomechanical Study of Serpentine Locomotion," Udine, Italy, Proc. 1st RoManSy Symp., pp 171-184.

2. Hirose, S., and Umetani, Y., 1976, "Kinematic Control of Active Cord Mechanism with Tactile Sensors," Proc. of 2nd Int. CISM-IFT Symp. On Theory and Practice of Robots and Manipulators, pp 241-252.

3. Hirose, S., and Morishima, A., 1990, "Design and Control of a Mobile Robot with an Articulated Body," International J. of Robotics Research, 9(2), pp 289-298.

4. Hirose, S., 1993, *Biologically Inspired Robots*, Oxford University Press, New York, NY.

5. Chirikjian, G. S., and Burdick, J. W., 1991, "Kinematics of Hyper Redundant Locomotion with Applications to Grasping," IEEE Int. Conf. on Robotics and Automation, Sacramento, CA, pp 720-727.

6. Burdick, J.W., and Radford, J., 1993, "A sidewinding Locomotion Gait for Hyper Redundant Robots," Atlanta, GA, IEEE Int. Conf. on Robotics and Automation, pp 101-106.

7. Ostrowski, J.P., 1995, "The Mechanics and Control of Undulatory Robotic Locomotion," Ph.D. thesis, California Institute of Technology, Pasadena, CA.

8. Ostrowski, J., and Burdick, J., 1998, "The Geometric Mechanics of Undulatory Robotic Locomotion," Int. J. Robotics Res., **120-D**(7), pp 683-701.

9 Shan, Y., and Koren, Y., 1993, "Design and Motion Planning of a Mechanical Snake," IEEE Trans. Sys. Man Cyb., **23**(4), pp 1091-1100.

10. Worst, R., and Linnemann, R., 1996, "Construction and Operation of a Snake-Like Robot," Proc. of IEEE Int. Joint Symp. Intel. Sys., Gaithersburg, MD, pp 164-169.

11. Klaassen, B., and Paap, K., 1999, "GMD-SNAKE2: A Snake-Like Robot Driven by Wheels and a Method for Motion Control," Proc. of IEEE Int. Conf. on Robotics and Auto.,Detroit, MI, pp 3014-3019.

12. Liu, H., Yan, G., and Ding, G., 2001, "Research on the Locomotion Mechanism of Snake-like robot," Int. symp. On Micromechatronics and Human Science, pp 183-188.

13. Dowling, K., 1997, "Limbless Locomotion: Learning to Crawl with a Snake Robot," Ph.D. thesis, Carnegie Mellon University, Pittsburgh, PA.

14. Dowling, K., 1999, "Limbless Locomotion: Learning to Crawl," Proc. IEEE Int. conf. Robotics and Auto., Detroit, MI, pp 3001-3006.

15. Ma, S., 1999, "Analysis of Snake Movement Forms for Realization of Snake-like Robot," Proc. IEEE Int. conf. Robotics and Auto., Detroit, MI, pp 3007-3013.

16. Spanos, P., Berka, R., and Tratskas, P., 2000, "Multisegment Large Space Robot: Concept and Design," J. Aerospace Eng., 13(4), pp 123-132.

17. Nilsson, M., 2004, "Serpentine locomotion on surfaces with uniform friction," Sendal, Japan, Proc. of IEEE Int. conf. on Intel. Robots Sys., pp 1751 – 1755.

18. Jalbert, J., Kashin, S., Ayers, J., 1995 "Design Considerations and Experiments on a Biologically-based Undulatory Lamprey-like AUV," Proc. Int. Symp. Unmanned Untethered Submersible Technology, Autonomous Undersea Systems Institute, Portsmouth, N.H., pp 124-138.

19. Saito, M., Fukaya, M., and Iwasaki, T., 2002, "Modeling, Analysis and Synthesis of Serpentine Locomotion with a Multilink Robotic Snake," IEEE Control Systems Magazine, **22**(1), pp.375-382.

20. Gravagne, I.A., and Walker, I.D., 2000, "Kinematics for Constrained Continuum Robots Using Wavelet Decomposition," Proc. 4th Intl. Conf. Exposition / Demonstration on Robotics for Challenging Situations and Environments, Albuquerque, New Mexico, pp 292-298.

21. Gravagne, I.A., and Walker, I.D., 2000, "On the Kinematics of Remotely-Actuated Continuum Robots," Proc. IEEE Int. conf. Robotics and Auto., San Francisco, CA, pp 2544-2550.

22. Gravagne, I.A., Rahn, C.D., and Walker, I.D., 2001, "Good Vibrations: A Vibration Damping Setpoint Controller for Continuum Robots," Proc. IEEE Int. conf. Robotics and Auto., Seoul, Korea, pp 3877-3883.

23. Gravagne, I.A., and Walker, I.D., 2002, "Uniform Regulation of a Multi-Section Continuum Manipulator," Proc. IEEE Int. conf. Robotics and Auto., Washington DC, pp 1519 – 1524.

24. Gravagne, I.A., and Walker, I.D., 2002, "Manipulability, Force, and Compliance Analysis for Planar Continuum Manipulators," IEEE Transactions on Robotics and Automation, **18**(3), pp. 263-273.

25. Gravagne, I.A., Rahn, C.D., and Walker, I.D., 2003, "Large Deflection Dynamics and Control for Planar Continuum Robots," IEEE/ASME Transactions on Mechatronics, **8**(2), pp. 299 – 307.

26. Douglas, J.F., Gasiorek, J.M., and Swaffield, J.A., 1995, *Fluid Mechanics*, Longman Scientific and Technical, Essex, England.

27. Logan, D.L., 1997, *A first course in the Finite Element Method Using Algor*, PWS Publishing Company, Boston, MA.